NACA RM A57H21

NACA

RESEARCH MEMORANDUM

THE USE OF A LEADING-EDGE AREA-SUCTION FLAP AND LEADING-

EDGE MODIFICATIONS TO IMPROVE THE HIGH-LIFT CHAR-

ACTERISTICS OF AN AIRPLANE MODEL WITH A WING

OF 45° SWEEP AND ASPECT RATIO 2.8

By David G. Koenig and Kiyoshi Aoyagi

Ames Aeronautical Laboratory
Moffett Field, Calif.

NATIONAL ADVISORY COMMITTEE
FOR AERONAUTICS
WASHINGTON

November 4, 1957
Declassified September 17, 1958

NATIONAL ADVISORY COMMITTEE FOR AERONAUTICS

RESEARCH MEMORANDUM

THE USE OF A LEADING-EDGE AREA-SUCTION FLAP AND LEADING-

EDGE MODIFICATIONS TO IMPROVE THE HIGH-LIFT CHAR-

ACTERISTICS OF AN AIRPLANE MODEL WITH A WING

OF 45° SWEEP AND ASPECT RATIO 2.8

By David G. Koenig and Kiyoshi Aoyagi

SUMMARY

An investigation was undertaken on an airplane model with drooped horizontal tail and a highly tapered wing of aspect ratio 2.8 and 45° sweep. The investigation was designed to determine what improvements in the control of leading-edge stall would be possible with the use of area suction on a leading-edge flap and with the leading-edge flap used with a modified or bulbous leading edge and a chord extension. Two spans of area-suction trailing-edge flap were tested. The tests were made at a Reynolds number of 8.9×10^6.

For both spans of trailing-edge flaps, the use of area suction on the leading-edge flap produced more constant stability near maximum lift than was obtained without area suction on the leading-edge flap in a previous investigation. The addition of the modified leading edge and the chord extension to the leading-edge flap with area suction increased the maximum lift coefficient of the order of 0.3 above that measured with the area-suction leading-edge flap alone.

INTRODUCTION

Results of tests on a large-scale model are reported in reference 1 with a wing of 45° sweep, aspect ratio 2.8, taper ratio 0.17, and with area suction applied to the trailing-edge flap. In that investigation, attempts were made to control leading-edge air-flow separation, in particular near the wing tip, by means of a plain leading-edge flap and a modified or bulbous leading edge. Although some improvements in the lift, drag, and stability characteristics of the model were made, it was found that the stall control effectiveness of the leading-edge flap with

or without the modified leading edge was seriously restricted by the
occurrence of air-flow separation behind the knee of the leading-edge
flap. The investigations of references 2 and 3 concerning two other
wing plan forms found boundary-layer control by porous area suction at
the knee of the flap extremely effective in delaying air-flow separation.
The question remains, however, whether area suction could be successfully
applied to the wing of reference 1 which had a smaller aspect ratio and
taper ratio and a thinner wing section than the wings of references 2
and 3.

The model of reference 1 was used in the present investigation but
had area suction applied to the knee of the leading-edge flap. The
objective of the tests was to develop leading-edge configurations which
would control stall and give higher values of $C_{L_{max}}$ and better longi-
tudinal stability. Most of the leading-edge configuration changes were
either (1) spanwise changes in leading-edge flap deflection and (2) changes
in spanwise extent of the modified leading edge, or combinations of these.
Limited testing was done with a chord extension installed on the outer
portion of the wing. The trailing-edge flaps with area suction remained
deflected during the tests and two spans of flap were tested.

NOTATION

a	chordwise location of forward edge of porous surface, deg (see figs. 3(b) and 3(c))
b	wing span, ft
c	chord, measured parallel to the plane of symmetry, ft
$\bar{c}$	mean aerodynamic chord, $\dfrac{2}{S}\displaystyle\int_{0}^{b/2} c^2 dy$, ft
C_D	drag coefficient, $\dfrac{drag}{qS}$
C_L	lift coefficient, $\dfrac{lift}{qS}$
$C_{L_{max}}$	value of C_L corresponding to lowest value of α for $\dfrac{dC_L}{d\alpha} = 0$
C_{L_s}	value of C_L at which the wing tip stalled
$C_{L_{stab}}$	value of C_L at which stability has begun to decrease

C_m pitching-moment coefficient computed about the quarter-chord point of the mean aerodynamic chord, $\dfrac{\text{pitching moment}}{q S \overline{c}}$

C_Q flow coefficient, $\dfrac{Q}{US}$

C_{Q_c} critical flow coefficient (value of C_Q at which C_L became approximately constant with increasing C_Q)

l chordwise extent of porous area, in. (see fig. 3(c))

l_t distance from the quarter-chord point of the mean aerodynamic chord to horizontal-tail reference line, ft

L.E.   leading edge

p free-stream static pressure, lb/sq ft

p_d average duct static pressure, lb/sq ft

p_l local-surface static pressure, lb/sq ft

P airfoil pressure coefficient, $\dfrac{p_l - p}{q}$

P_d average duct pressure coefficient, $\dfrac{p_d - p}{q}$

q free-stream dynamic pressure, lb/sq ft

Q volume of air removed through porous surface, based on standard density, cu ft/sec

R radius

S wing area, sq ft

T airplane thrust, lb

T.E.   trailing edge

U free-stream velocity, ft/sec

V airplane velocity, knots

V_{min} minimum flying speed, knots

V_{stab} velocity at which static stability has begun to decrease, knots

W   weight of airplane, lb

y   perpendicular distance from plane of symmetry, ft

z   perpendicular distance above the extended wing chord plane, ft

α angle of attack, deg

δ_n leading-edge flap deflection, measured in plane normal to the
             hinge line, deg

η spanwise distance, $\dfrac{y}{b/2}$

ρ density, slugs/cu ft

Λ sweep angle, deg

Δp pressure drop across porous material, lb/sq ft

MODEL AND APPARATUS

Model

The model as mounted in the 40- by 80-foot wind tunnel is shown in
figure 1 and is identical in most respects to the one reported on in
reference 1. A drawing of the model is shown in figure 2, and additional
geometric data are given in table I. The wing of the model had a sweep
of the quarter-chord line of 45°, an aspect ratio of 2.8, and a taper
ratio of 0.17. Airfoil sections parallel to the model symmetrical center
line were modified NACA 0005-63 sections, the coordinates of which are
listed in table II. The modification consisted of a straight-line fairing
from the 67-percent chord station to the trailing edge.

A leading-edge flap was installed on the wing and was hinged near
the lower surface of the wing. Area suction could be applied to the knee
of the leading-edge flap. The leading-edge flap was hinged at the 12-
percent chord line (streamwise) and consisted of three spanwise sections
with breaks parallel to the model plane of symmetry at 0.21, 0.40, 0.70,
and 1.0 of the wing semispan. A particular flap deflection combination
will hereinafter be referred to in the order 30°, 50°, 60°, which will
refer to 30° for η = 0.21 to 0.40, 50° for η = 0.40 to 0.70, and 60°
for η = 0.70 to 1.0.

A small-span and a large-span trailing-edge flap were used during
the tests. The small-span flap had a constant chord and extended from
η = 0.21 to 0.46. The large-span flap was formed by combining the

small-span flap with an outboard flap which had a constant 25-percent chord and extended from $\eta = 0.46$ to 0.66. It should be noted that a discontinuity of the hinge lines of the outboard and inboard flaps at $\eta = 0.46$ caused a small chordwise slit in the large-span flap at this point but no attempt was made to seal this slit. A flap deflection of 60° was maintained throughout the tests.

The fuselage and side-inlet duct configurations were identical to those of the model of reference 1. A swept horizontal tail which was drooped 15° was mounted with its root chord 0.21 of the wing semispan above the extended wing-chord plane. The tail was set at 0° incidence for all tests.

Boundary-Layer Control System

Duct and pumping system.- The suction systems employed on the leading- and trailing-edge flaps are shown in figure 3(a). Air was drawn from the flaps through the wing ducts and plenum chambers into the blowers and then was exhausted through the exhaust ducts beneath the fuselage. The pumps were modified aircraft engine superchargers driven by variable-speed electric motors. The flow quantity was obtained by measuring the pressure difference between the plenum chamber and the inlet pipe to the blower; this system was calibrated against standard ASME intake orifices. Wing duct pressure measurements were obtained from static pressure taps inside the duct located at 0.25, 0.37, 0.52, 0.62, 0.75, and 0.90 of the wing semispan.

Porous surface.- The flaps were constructed with the porous surface in the vicinity of the knee of the flaps as shown in figure 3(b) and (c) for the leading- and trailing-edge flaps, respectively. The porous material was composed of 0.008-inch-thick electroplated metal mesh sheets, 11-percent porous with 4225 holes per square inch, backed with 1/16-inch-thick white wool felt. The permeability of the felt with the metal mesh sheet for the leading- and trailing-edge flaps is shown in figure 3(d) and reference 1 (fig. 3(c)), respectively. Chordwise extent and position of the porous opening were controlled by covering portions of the porous surface with 0.003-inch-thick nonporous tape. The porous openings used in the tests are shown in table III for both leading- and trailing-edge flaps. Aside from brief tests with the leading-edge flap at a constant deflection from $\eta = 0.21$ to 1.0, the porous area on the leading-edge flap was always sealed between $\eta = 0.21$ and 0.40.

Wing Modifications

During the investigation, a modified leading edge and a chord extension were installed on the wing leading edge. Details of these leading-edge modifications are shown in figure 4, and contour ordinates are listed in table IV.

Modified leading edge.- The modified leading edge was obtained by increasing the leading-edge radius from 0.36 (for the basic wing) to 0.90 percent of the wing chord (normal to the leading edge) with a slight amount of camber near the leading edge. Several spanwise extents of modified leading edge were tested which extended from the wing tip inboard to points coinciding with leading-edge flap breaks at $\eta = 0.4$, 0.6, and 0.7.

Chord extension.- The plain chord extension was obtained by extending the plain leading edge forward (see fig. 4(b)) from $\eta = 0.7$ to 1.0. The resulting chordwise contour had a discontinuity in slope where the chord extension met the wing surface. A modified leading edge similar in contour to that described above was installed on the plain chord extension for some of the tests.

TESTING AND PROCEDURE

Force and moment data were obtained for the model through an angle-of-attack range of -4° to 28°. The model configurations for which force and moment data were obtained are listed in table V. All tests were made at a Reynolds number of 8.9×10^6, based on the mean aerodynamic chord. This Reynolds number corresponded to a free-stream dynamic pressure of 15 pounds per square foot and a Mach number of 0.10.

Tests at Variable Angles of Attack

For the model with the small-span trailing-edge flap deflected 60°, with area suction on both leading- and trailing-edge flaps, the following leading-edge configurations were investigated: (1) the leading-edge flap with plain leading edge deflected 50°, part span ($\eta = 0.4 - 1.0$) or full span ($\eta = 0.21 - 1.0$), (2) the leading-edge flap deflected various amounts along the wing span, (3) the leading edge modified for various spanwise extents combined with the more effective leading-edge flap deflection configurations, and (4) the chord extension mounted on the deflected leading-edge flap both with and without the modified leading edge. Other tests were made for the model with the large-span trailing-edge flap deflected 60° both with and without area suction, and for the

model with the small-span trailing-edge flap without area suction. The leading-edge configurations used in these latter tests were those found most effective in controlling flow separation with the small-span area-suction flap.

During these tests, C_Q for the leading-edge flap was increased with increasing angle of attack so that the values of C_Q were set well above C_{Q_c} for all portions of the angle-of-attack range. It was found that as long as C_Q was greater than C_{Q_c} at each angle of attack, the force and moment characteristics for a given model configuration were independent of suction flow quantity and chordwise extent of porous opening.

Throughout the test, C_Q for the trailing-edge flap was held at values of approximately 0.0006 and 0.0012 for the small- and large-span flaps, respectively. These values were well above C_{Q_c} for the respective flaps.

Tests With Variable Suction Flow at Constant Angle of Attack

The leading-edge flap suction flow quantity was varied at constant values of angle of attack near that for $C_{L_{max}}$ for some of the more effective leading-edge configurations tested. Several chordwise extents and locations of the porous openings were investigated, two of which are reported herein.

Corrections to Data

All data corrections were identical to those described in reference 1.

RESULTS AND DISCUSSION

Table V may be used as an index to figures 5 through 13, in which force and moment data obtained during the present investigation are presented. In several of the figures, results are compared with those obtained with two of the most effective wing configurations previously tested (ref. 1).

Force and Moment Characteristics of the Model

Effect of area suction on the leading-edge flap.- It was noted in reference 1 that with no area suction more than 40° nose flap deflection was ineffective in controlling leading-edge flow separation. The effect of applying area suction to the leading-edge flap deflected 50° over the best spanwise extent found in reference 1 is shown in figure 5. The onset of flow separation on the outer portion of the wing is indicated by the initial and abrupt changes in model stability as shown by the C_m versus C_L curves of figure 5. It is shown that area suction was instrumental in delaying this flow separation approximately 5° in angle of attack or 0.2 in C_L.

Comparison of the full-span and part-span leading-edge flap.- As shown by the data of figure 6 with area suction on the leading-edge flap, a higher value of $C_{L_{max}}$ could be obtained with a part-span leading-edge flap than with a full-span flap. However, the use of the part-span leading-edge flap resulted in marked longitudinal instability at large values of C_L. As was shown in the investigation of reference 1, these differences between the part-span and full-span flap were also obtained without area suction on the leading-edge flap.

Spanwise adjustment of leading-edge stall control.- The results just discussed indicated that while area suction on a leading-edge flap was an effective means of leading-edge stall control, the spanwise distribution of stall control would have a strong effect on $C_{L_{max}}$ and longitudinal stability. Determination of the stall control configurations giving the highest values of $C_{L_{max}}$ while retaining longitudinal stability was a trial and error process. The leading-edge configurations used consisted of the following either alone or in combination: spanwise changes in leading-edge flap deflection, a modified leading edge of several spanwise extents, and a chord extension installation. Force and moment data for the model configurations tested during this phase of the investigation are presented in figures 7 through 10 for the model with the small-span trailing-edge flap and in figures 11 and 12 for the large-span flap.

Summary of results with the small-span trailing-edge flap: Values of $C_{L_{max}}$ and stability criteria are listed in the following table for the more significant model configurations with the small-span trailing-edge flap deflected. The next to last column answers the question whether or not the pitching-moment variation above the break in the curve was stable and in the last column are values of the lowest C_L at which stability changes occur.

Figure no.	Leading-edge configuration		$C_{L_{max}}$	Stable	$C_{L_{stab}}$
	Leading-edge flap	Wing leading edge			
6	$0°,50°,50°$	Plain	1.41	No	1.10
6	$50°,50°,50°$	Plain	1.23	No	1.20
9(b)	$30°,50°,60°$	Plain	1.31	No	1.30
7	$0°,50°,50°$	Modified ($\eta = 0.7$-1.0)	1.46	No	1.11
8	$30°,40°,50°$	Modified ($\eta = 0.7$-1.0)	1.39	No	1.36
8	$30°,50°,50°$	Modified ($\eta = 0.7$-1.0)	1.51	Nearly neutral	1.50
9(b)	$30°,50°,60°$	Modified ($\eta = 0.7$-1.0)	1.49	No	1.47
9(b)	$30°,50°,60°$	Modified ($\eta = 0.6$-1.0)	1.58	Nearly neutral	1.51
10(a)	$30°,50°,60°$	Chord extension	1.50	No	1.38

As had been expected, it became immediately evident from the tests that, in general, extremely large spanwise changes in leading-edge stall control requirements existed for the wing, the most effective control being required on the outer portion of the wing or near the tips. It was also found, however, that, as more effective stall control was applied to the outer portion of the wing, it became necessary to augment stall control on the inner portion of the wing.

Comparison with previous tests: In the present tests, the most effective configuration found from a standpoint of $C_{L_{max}}$ and model stability consisted of the 30, 50, 60 leading-edge flap deflection with the modified leading-edge installed near the wing tip. Results of tests with this flap deflection with and without the modified leading edge and results of tests with the most effective leading-edge configuration found in the investigation of reference 1 are presented in figure 13. Along with the improvement in $C_{L_{max}}$ obtained with the more effective wing configurations in the present tests, a major improvement was obtained in model stability in the angle-of-attack range close to that of $C_{L_{max}}$.

Values of C_{L_S}[1] obtained from both investigations are presented in figure 14 for various values of leading-edge flap deflection with and without the modified leading edge. These data show that the change in C_{L_S} due to the modified leading edge was constant throughout the range of leading-edge flap deflections considered. In addition, results shown in the figure demonstrate that area suction was needed to increase C_{L_S} for flap deflections above $\delta_n = 15°$ and $30°$ for the modified leading edge and plain leading edge, respectively. The use of area suction in the present investigation insured further improvement with increasing flap deflection up to $\delta_n = 60°$, the largest leading-edge flap deflection investigated.

---

[1]Values of C_L for tip stall, C_{L_S}, determined by pressure measurements are presented in figure 14 together with values of C_L at the occurrence of abrupt stability changes. It is noted that, in general, $C_{L_S} = C_{L_{stab}}$.

Chord extension compared with the modified leading edge: From the data of figure 10(b), it is evident that for equivalent spanwise locations ($\eta = 0.7 - 1.0$) the chord extension produced the same value of $C_{L_{max}}$ as did the modified leading edge. However, with the chord extension, destabilizing pitching-moment variations were experienced at values of C_L lower than with the modified leading edge.

Summary of results with the large-span trailing-edge flap: The tests with the large-span trailing-edge flap deflected were limited to those leading-edge configurations found most effective with the small-span trailing-edge flap. Force and moment data obtained with the large-span flap are presented in figures 11 and 12.

Values of $C_{L_{max}}$ as well as values of C_L for initial stability break are presented in the following table for the cases of both trailing-edge flap spans, with and without suction on the trailing-edge flap.

| Figure no. | Trailing-edge flap | | Leading-edge flap deflection | Wing leading edge | $C_{L_{max}}$ | $C_{L_{stab}}$ |
	Span	Suction				
9(b)	Small	On	30°,50°,60°	Plain	1.31	1.30
12(b)	Large	On		Plain	1.34	1.30
9(b)	Small	On		Modified ($\eta = 0.6$-1.0)	1.58	1.51
12(b)	Large	On		Modified ($\eta = 0.6$-1.0)	1.64	1.54
9(a)	Small	Off		Modified ($\eta = 0.6$-1.0)	1.45	1.30
12(a)	Large	Off	↓	Modified ($\eta = 0.6$-1.0)	1.46	1.25

Comparison of the above values indicates that in general only slight, if any, improvement in $C_{L_{max}}$ and $C_{L_{stab}}$ were obtained by increasing the flap span. There was a tendency for the stability break at or near $C_{L_{max}}$ to be unstable, with either span of trailing-edge flap, particularly with area suction on. Comparisons of the data of figures 9 and 12 show that the severity of this unstable break was much greater for the model with the large-span trailing-edge flap.

It seems evident then that more effective leading-edge stall control devices than those used in the present tests must accompany the use of a larger span flap before the lift advantage of the flap in the high lift range (high angle of attack) would become significant.

Low-Speed Level Flight Performance

Changes in stall control made in the present investigation may be evaluated in part with reference to figure 15. In that figure, variations of thrust required for level flight with airspeed[2] are presented for leading-edge configurations which represent various degrees of leading-edge stall control obtained during the tests. Approximate values of minimum flying speed (defined as the velocity corresponding to $C_{L_{max}}$), V_{min}, 1.30 V_{min}, and the limiting speed for near constant stability, V_{stab}, are listed in the following table.

Small-span flap - suction on					
Leading-edge flap			V_{min}	1.30 V_{min}	V_{stab}
Deflection	Suction	Wing leading edge			
$0°,40°,40°$	Off	Plain	111	144	138
$30°,50°,60°$	On	Plain	114	148	115
$30°,50°,60°$	On	Chord extension	104	135	112
$30°,50°,60°$	On	Modified L.E. ($\eta = 0.6$-1.0)	103	134	107
Large-span flap - suction on					
$30°,50°,60°$	On	Plain	115	150	118
$30°,50°,60°$	On	Modified L.E. ($\eta = 0.6$-1.0)	102	133	108

Suction Requirements for the Leading-Edge Flap

Suction flow requirements.- As noted earlier, for most of the tests, the suction quantity used at the leading edge was held well above that required to maintain attached flow. For the best leading-edge arrangement found, tests were made at an angle of attack close to $C_{L_{max}}$ to

[2]The data are presented as values of T/S and V, where:

$$\frac{T}{S} = \frac{W}{S} \frac{C_D}{C_D \sin \alpha + C_L' \cos \alpha} , \qquad V = 0.592 \sqrt{\frac{2}{\rho} \left(\frac{W/S}{C_L' + C_D \tan \alpha} \right)}$$

and

$$C_L' = C_L + \frac{\overline{c}}{l_t} C_m$$

determine the minimum value of C_Q required to attach the flow. At lower angles, a lesser value would be required, as shown in references 2 and 3 and as indicated by the data of figure 16. One adjustment of position and extent of porous area was made to determine if lower values of C_Q were possible. The results of these studies are shown in figure 17. The lowest value of C_Q for flow attachment was about 0.0010. That some reduction was possible indicates that lower values might be achieved with such methods as changes in spanwise and chordwise extent of porous surface permeability.

Duct and minimum external pressure.- Spanwise variation in duct and minimum external pressure are presented in figure 18 for the porous area configurations considered in figure 17. An examination of figures 17 and 18 shows that the duct pressures may be increased to, or slightly above, the minimum external pressure near the wing tip before any appreciable reduction in wing lift occurred for the model with the larger porous opening (porous area 1). With the smaller porous opening, considerably more suction pressure was required to maintain attached air flow.

CONCLUDING REMARKS

From the present investigation concerning the use of area suction on the leading-edge flap as well as from tests on additional wing configurations embodying a modified or bulbous leading edge and a chord extension, the following results were found for two spans of trailing-edge flaps.

The use of area suction on the knee of the leading-edge flap resulted in nearly constant stability up to angles of attack near that of $C_{L_{max}}$. There was no marked increase in $C_{L_{max}}$ with the use of the area-suction leading-edge flap with the plain leading edge. Increases in $C_{L_{max}}$ of the order of 0.3 were obtained when wing modifications such as a bulbous leading edge or a chord extension, installed principally near the wing tip, were combined with the area-suction leading-edge flap.

Ames Aeronautical Laboratory
        National Advisory Committee for Aeronautics
            Moffett Field, Calif., Aug. 21, 1957

REFERENCES

1. Koenig, David G., and Aoyagi, Kiyoshi: Large-Scale Wind-Tunnel Tests of an Airplane Model With a 45° Sweptback Wing of Aspect Ratio 2.8 With Area Suction Applied to Trailing-Edge Flaps and With Several Wing Leading-Edge Modifications. NACA RM A56H08, 1956.

2. Holzhauser, Curt A., and Martin, Robert K.: The Use of a Leading-Edge Area-Suction Flap to Delay Separation of Air Flow From the Leading Edge of a 35° Sweptback Wing. NACA RM A53J26, 1953.

3. Holzhauser, Curt A., Martin, Robert K., and Page, V. Robert: Application of Area Suction to Leading-Edge and Trailing-Edge Flaps on a 44° Swept-Wing Model. NACA RM A56F01, 1956.

TABLE I.- GEOMETRIC DATA

```
Wing
  Area, sq ft . . . . . . . . . . . . . . . . . . . . . . . . . . . 334.8
  Span, ft . . . . . . . . . . . . . . . . . . . . . . . . . . . . 30.62
  Mean aerodynamic chord, ft . . . . . . . . . . . . . . . . . . . 12.77
  Root chord, ft . . . . . . . . . . . . . . . . . . . . . . . . . 18.69
  Aspect ratio . . . . . . . . . . . . . . . . . . . . . . . . . .   2.8
  Taper ratio . . . . . . . . . . . . . . . . . . . . . . . . . .   0.17
  Sweep angle, deg
    Leading edge . . . . . . . . . . . . . . . . . . . . . . . . . 51.70
    Quarter-chord line . . . . . . . . . . . . . . . . . . . . . . 45.36
    Trailing edge . . . . . . . . . . . . . . . . . . . . . . . . 14.18
Small-span flap (T.E.)
  Area, sq ft . . . . . . . . . . . . . . . . . . . . . . . . . . 20.44
  Flap span, percent wing semispan . . . . . . . . . . . . . . . . 25.0
  Constant streamwise chord, ft . . . . . . . . . . . . . . . . .  2.67
  Sweep angle of hinge line, deg . . . . . . . . . . . . . . . . . 14.18
Large-span flap (T.E.)
  Area, sq ft . . . . . . . . . . . . . . . . . . . . . . . . . . 35.73
  Flap span, percent wing semispan . . . . . . . . . . . . . . . . 45.0
  Sweep angle of hinge line, deg
    η = 0.21 - 0.46 . . . . . . . . . . . . . . . . . . . . . . . 14.18
    η = 0.46 - 0.66 . . . . . . . . . . . . . . . . . . . . . . . 26.84
Fuselage
  Length, ft . . . . . . . . . . . . . . . . . . . . . . . . . . . 62.50
  Maximum width, ft . . . . . . . . . . . . . . . . . . . . . . .  4.50
  Fineness ratio in wing chord plane . . . . . . . . . . . . . . . 13.9
Horizontal tail (drooped 15°)
  S_t/S . . . . . . . . . . . . . . . . . . . . . . . . . . . . . 0.197
  b_t/b . . . . . . . . . . . . . . . . . . . . . . . . . . . . .  0.54
  l_t/c̄ . . . . . . . . . . . . . . . . . . . . . . . . . . . . .  1.51
  Aspect ratio . . . . . . . . . . . . . . . . . . . . . . . . . . 4.16
  Taper ratio . . . . . . . . . . . . . . . . . . . . . . . . . . 0.296
  Sweep angle of quarter-chord line, deg . . . . . . . . . . . . . 39.4
```

TABLE II.- COORDINATES OF THE NACA 0005 (MODIFIED) SECTION

PARALLEL TO MODEL SYMMETRICAL CENTER LINE

Station, percent chord	Ordinate, percent chord
0	0
1.25	.789
2.50	1.089
5.00	1.481
7.50	1.750
10.00	1.951
15.00	2.228
20.00	2.391
25.00	2.476
30.00	2.501
40.00	2.419
50.00	2.206
60.00	1.902
67.00	1.650
70.00	1.500
80.00	1.000
90.00	.500
100.00	0

L.E. radius: 0.275-percent chord

TABLE III.- POROUS AREA CONFIGURATIONS USED IN THE INVESTIGATIONS

(a) Leading-edge flap

Porous area no.	a, deg and l, in.	Station, η					
		0.21	0.4	0.6	0.7	0.7	1.0
1	a	20	20	20	20		20
	l	4.6	3.2	3.1	1.7		1.2
2	a		25	25	25	24	24
	l		2.2	1.5	1.2	3.1	1.6

(b) Trailing-edge flap

Porous area no.	a, deg and l, in.	Station, η			
		Inboard flap		Outboard flap	
		0.21	0.46	0.46	0.66
4	a	30	30	Undeflected	
	l	2	2		
5	a	24	24	Undeflected	
	l	3	3		
6	a	24	24	24	24
	l	3	3	3	3

TABLE IV.- COORDINATES OF SEVERAL MODIFIED LEADING-EDGE SECTIONS

PERPENDICULAR TO LEADING EDGE OF PLAIN WING

Modified leading edge on wing					
Station, percent chord	Ordinate, percent chord		Station, percent chord	Ordinate, percent chord	
	Upper surface	Lower surface		Upper surface	Lower surface
0	-0.60	-0.60	2.00	1.06	-1.71
.05	-.29	-.89	2.50	1.21	-1.71
.10	-.18	-1.01	3.00	1.38	-1.70
.25	.07	-1.22	3.50	1.42	-1.68
.50	.35	-1.42	4.00	1.49	-1.67
.75	.53	-1.54	4.50	1.57	-1.66
1.25	.80	-1.65	5.00	1.64	-1.64
Modified leading edge on plain chord extension					
-5.40	-0.60	---	-3.60	---	-1.65
-5.30	-.17	-0.99	-3.20	0.97	-1.62
-5.20	-.02	-1.16	-3.00	1.02	-1.61
-5.00	.21	-1.35	-2.00	1.15	-1.46
-4.60	.49	-1.55	-1.00	1.23	---
-4.20	.67	-1.64	-.92	---	-1.24

Plain chord extension[1]	
Station, percent chord	Ordinate, percent chord
-4.83	0
-4.75	.23
-4.60	.39
-4.40	.53
-4.20	.64
-3.90	.78
-3.00	1.03
-2.00	1.15
-1.00	1.23
·1.00	1.35
3.99	1.50

[1]Symmetrical section

TABLE V.- INDEX TO FIGURES WITH FORCE AND MOMENT DATA

Figure no.	T.E. flap Span	T.E. flap Suction	L.E. Flap Deflection	L.E. Flap Suction[1]	Modified L.E. (spanwise extent)	Chord extension
5	Small	On	$0°,40°,40°$[2] $0°,50°,50°$	Off On	None None	Off
6	Small	On	$0°,50°,50°$ $50°,50°,50°$	On	None	
7	Small	On	$0°,50°,50°$ $0°,50°,50°$ $30°,50°,50°$		$\eta = 0.7 - 1.0$ $0.21 - 0.4$ & $0.7 - 1.0$ $0.7 - 1.0$	
8	Small	On	$30°,40°,50°$ $30°,50°,50°$ $30°,50°,60°$		$\eta = 0.7 - 1.0$	
9(a)	Small	Off	$30°,50°,60°$		$\eta = 0.7 - 1.0$ $0.6 - 1.0$	
9(b)	Small	On	$30°,50°,60°$		None $\eta = 0.7 - 1.0$ $0.6 - 1.0$	
10(a)	Small	On	$30°,50°,60°$		None	Off On
10(b)	Small	On	$30°,50°,60°$		$\eta = 0.7 - 1.0$	Off On
10(c)	Small	On	$30°,50°,60°$		$\eta = 0.6 - 1.0$	Off On
11(a)	Large	Off	$0°,50°,60°$ $15°,50°,60°$ $30°,50°,60°$		$\eta = 0.4 - 1.0$	Off
11(b)	Large	On	$0°,50°,60°$ $15°,50°,60°$ $30°,50°,60°$		$\eta = 0.4 - 1.0$	
12(a)	Large	Off	$30°,50°,60°$		None $\eta = 0.7 - 1.0$ $0.6 - 1.0$ $0.4 - 1.0$	
12(b)	Large	On	$30°,50°,60°$		None $\eta = 0.7 - 1.0$ $0.6 - 1.0$ $0.4 - 1.0$	
13(a)	Small	On	$0°,40°,40°$[2] $30°,50°,60°$	Off On	None	
13(b)	Small	On	$0°,40°,40°$[2] $30°,50°,60°$	Off On	$\eta = 0.4 - 1.0$	

[1] Extending from $\eta = 0.4 - 1.0$
[2] Data from reference 1

A-20739.1

Figure 1.- Photograph of the model mounted in the Ames 40- by 80-foot
wind tunnel.

75-percent c line, hinge line for
outboard T.E. flap
    12-percent c line, hinge
    line for L.E. flap

3.18

15.31

48.9°

3.22
4.50

10.09
7.04

51.7°   c̄=12.77

5.84

L.E. flap breaks
at .21, .4,
.7 semispans

2.67

c̄/4

42.6°

4.30

22.33   10.59   19.24

Horizontal tail
reference line
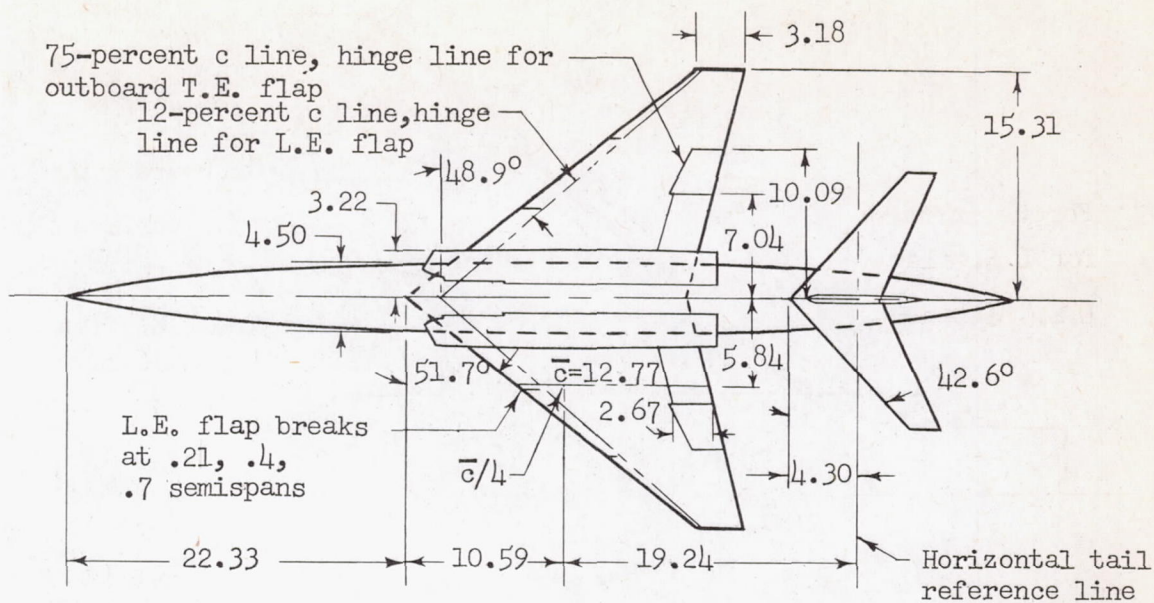
All dimensions in feet
unless otherwise noted

Intersection of vertical
and horizontal tail planes

45.0°

4.12

10.82

3.17

62.50

10.51

Exhaust ducts

8.57   15°
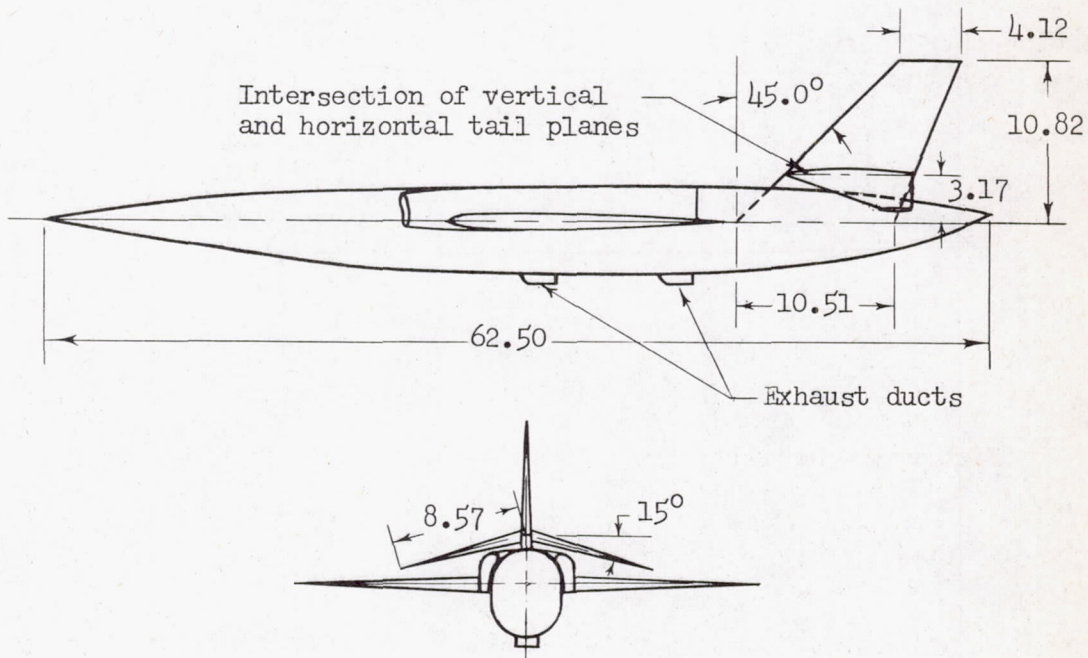
Figure 2.- Dimensional details of the model.

Porous surface
for L.E. flap

L.E. flap duct

Outboard T.E. flap

Porous surface for
T.E. flap

Inboard T.E. flap

T.E. flap duct

L.E. plenum chamber

L.E. motor-
blower
unit

T.E. plenum chamber

T.E. motor-blower
unit

Wing-chord plane

Exhaust ducts
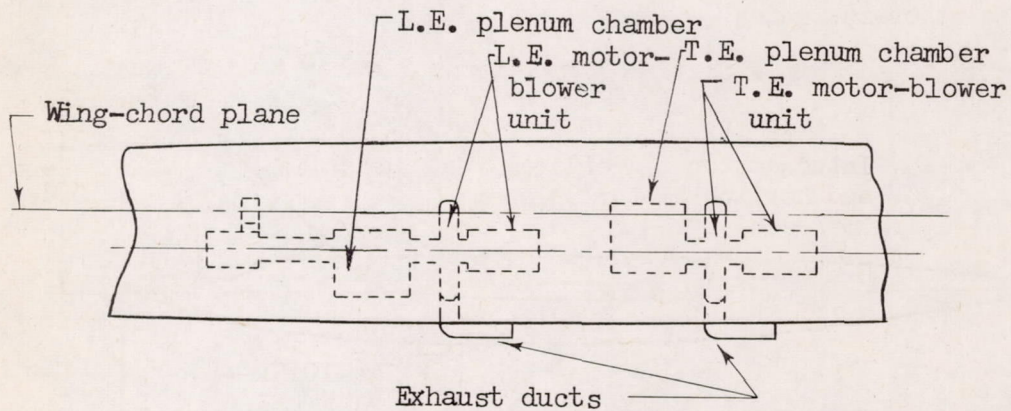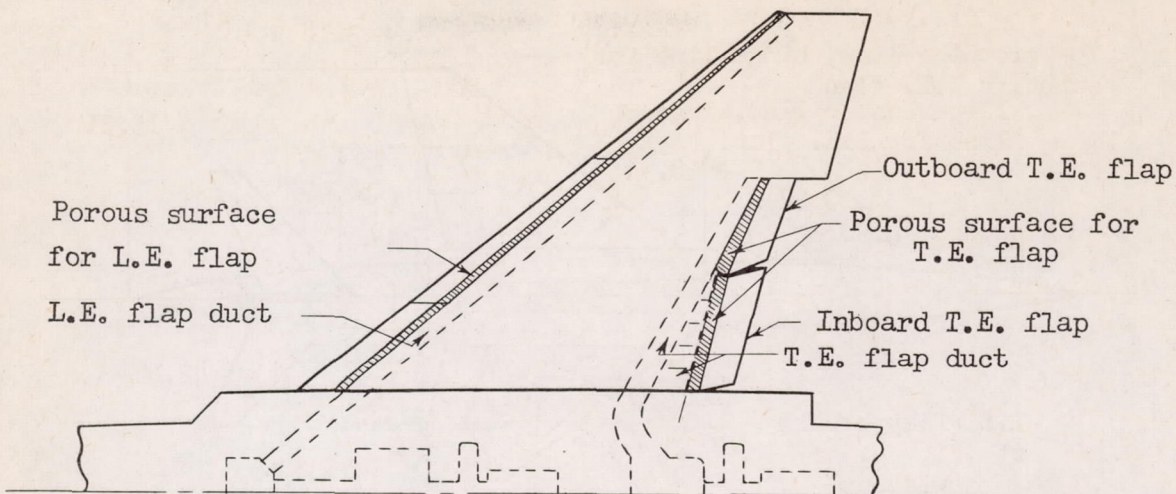
(a) Details of duct and pumping system.

Figure 3.- Details of porous area, duct, and pumping system.

Reference line
normal to upper
surface

Porous surface (constant porosity)
metal mesh backed with wool felt
See figure 3(d)

.003-inch-thick pressure-
sensitive tape

l, inches

a, degrees

L.E. flap

Duct

L.E. flap hinge

(b) Leading-edge flap. Section shown perpendicular to the hinge line.

Reference line, normal
to upper surface
a, degrees

Porous surface (constant
porosity)metal mesh
backed with wool felt.
See reference 1 for
porosity.

l, inches

.003-inch-thick pressure
sensitive tape
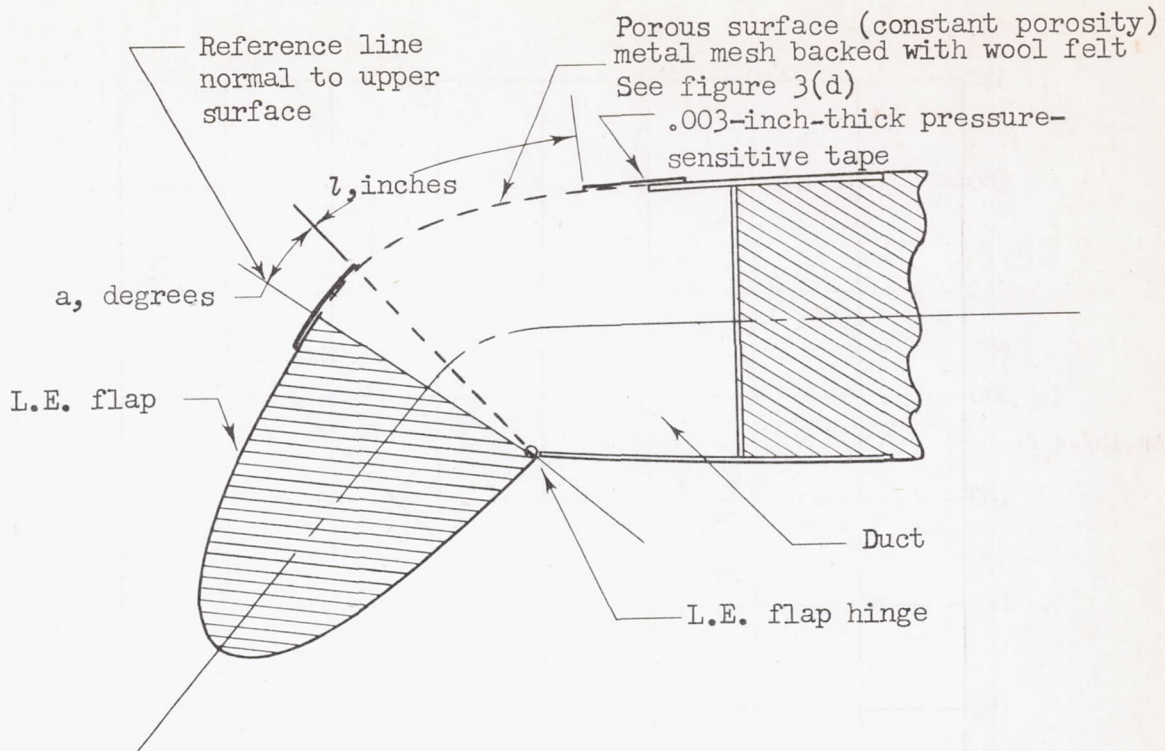
T.E. flap hinge
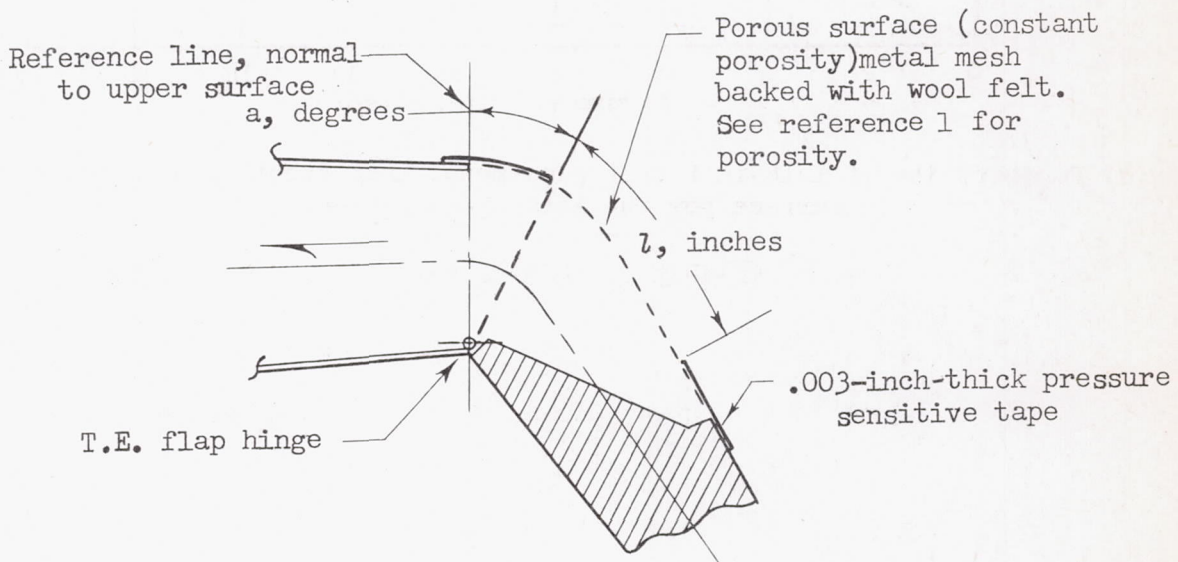
(c) Trailing-edge flap. Section shown perpendicular to the hinge line.

Figure 3.- Continued.
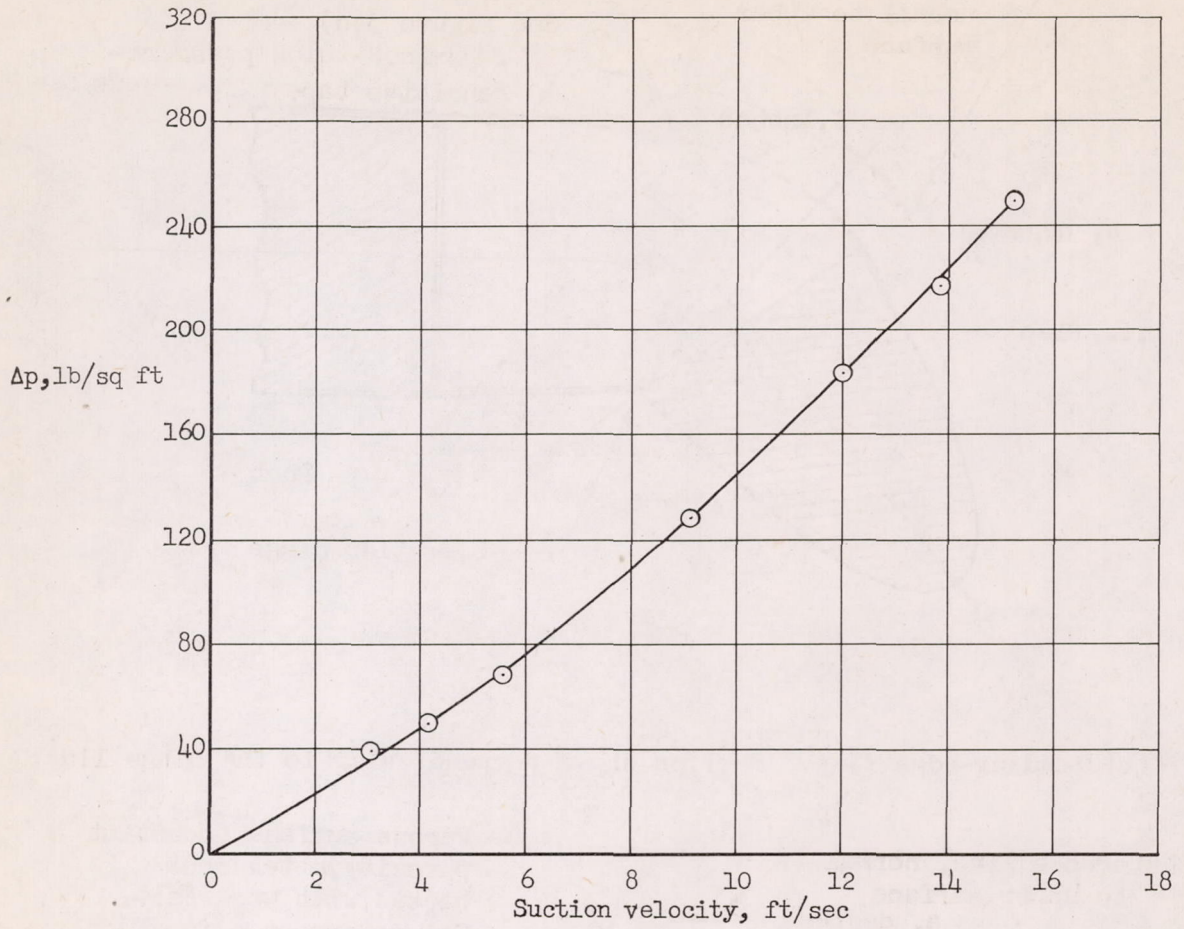
(d) Permeability of 1/16-inch felt plus metal mesh sheet used as porous surface for the leading-edge flap.

Figure 3.- Concluded.
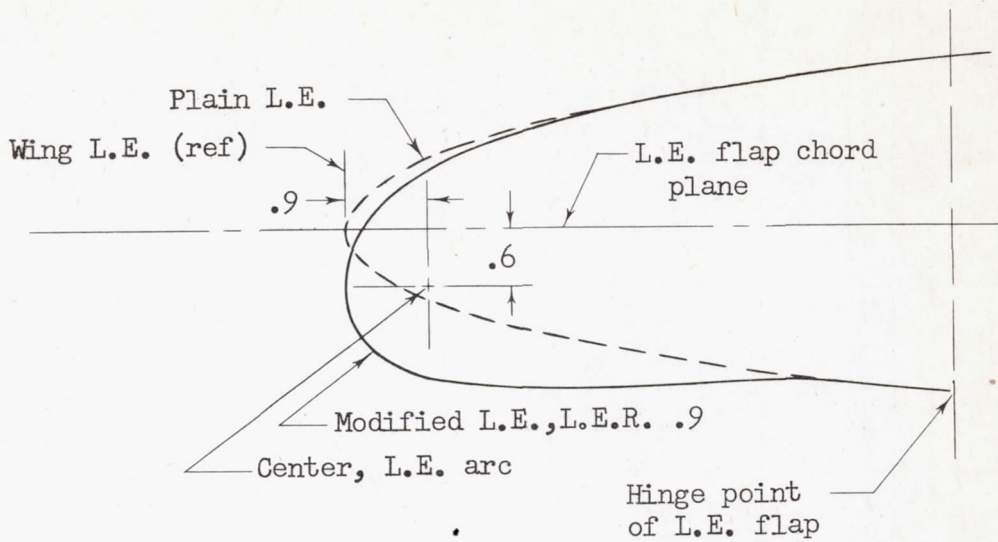
(a) Modified leading edge.
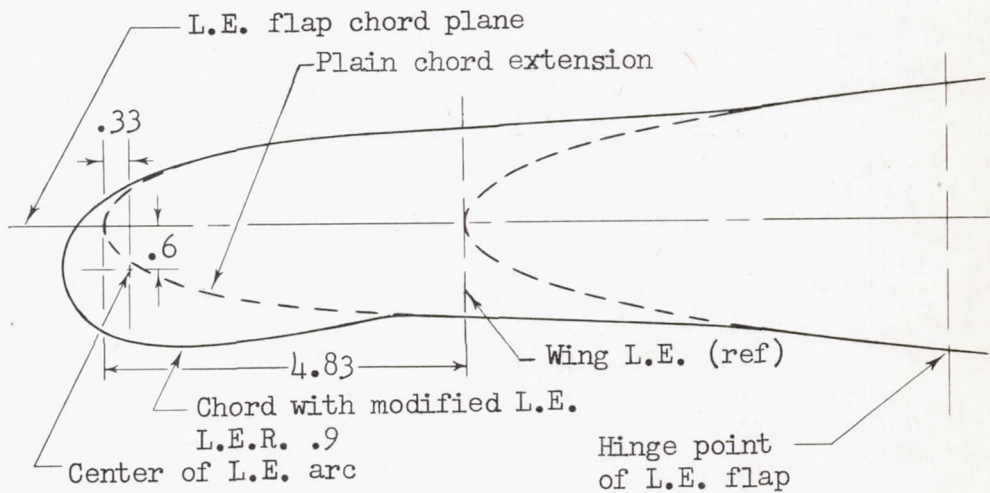
(b) Chord extension.

Figure 4.- Leading-edge modification used in the investigation. All sections perpendicular to the wing leading edge. All dimensions are in percent chord.
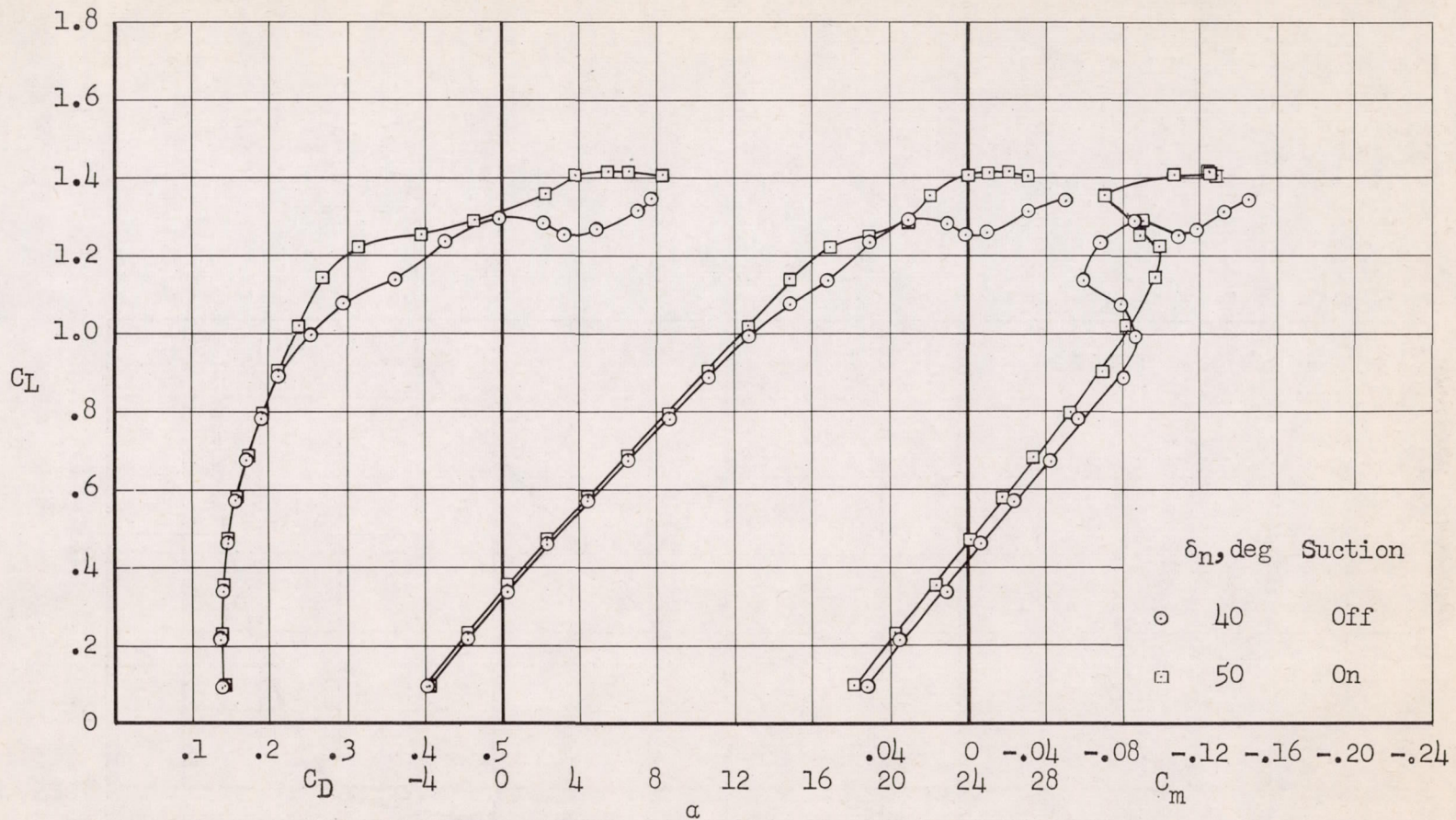
Figure 5.- Aerodynamic characteristics of the model with a part-span leading-edge flap (η = 0.4 - 1.0) for the model with the small-span trailing-edge flap; area suction on the trailing-edge flap; data for δ_n = 40° were taken from investigation of reference 1.
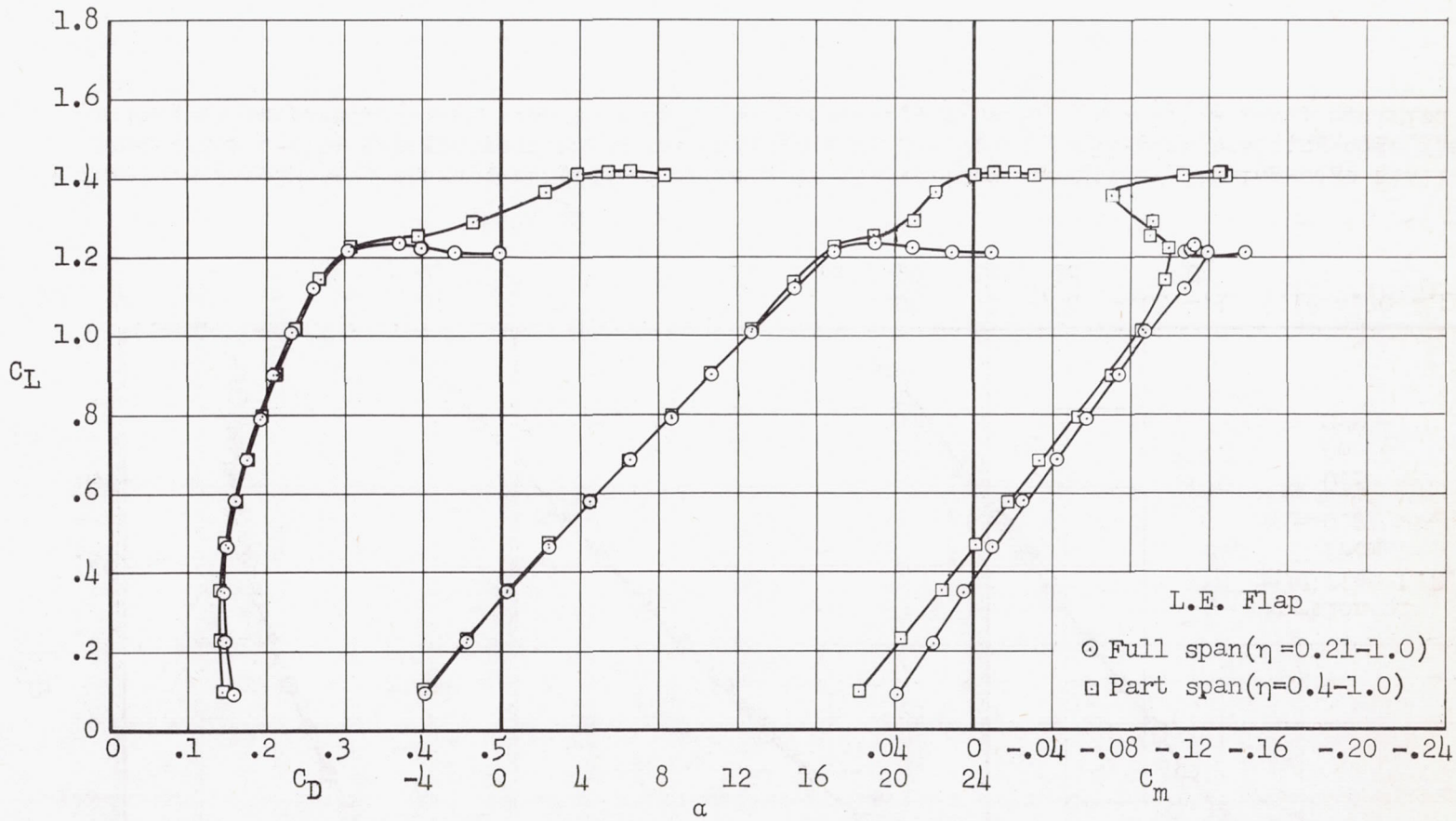
Figure 6.- Effect of a change in leading-edge flap span on the aerodynamic characteristics of the model with the small-span trailing-edge flap; suction on leading-edge flap; $\delta_n = 50°$; plain leading edge; suction on trailing-edge flap.
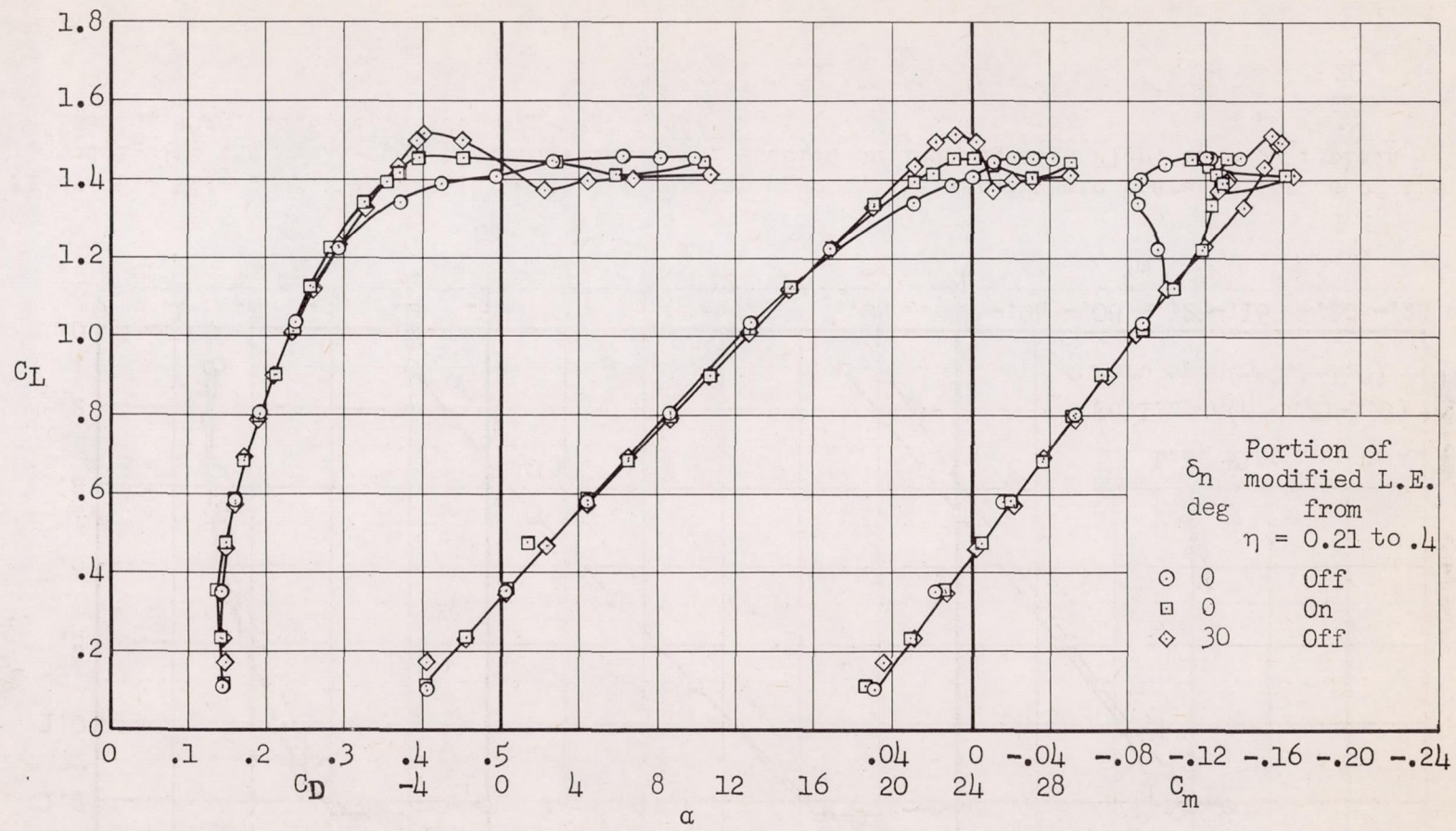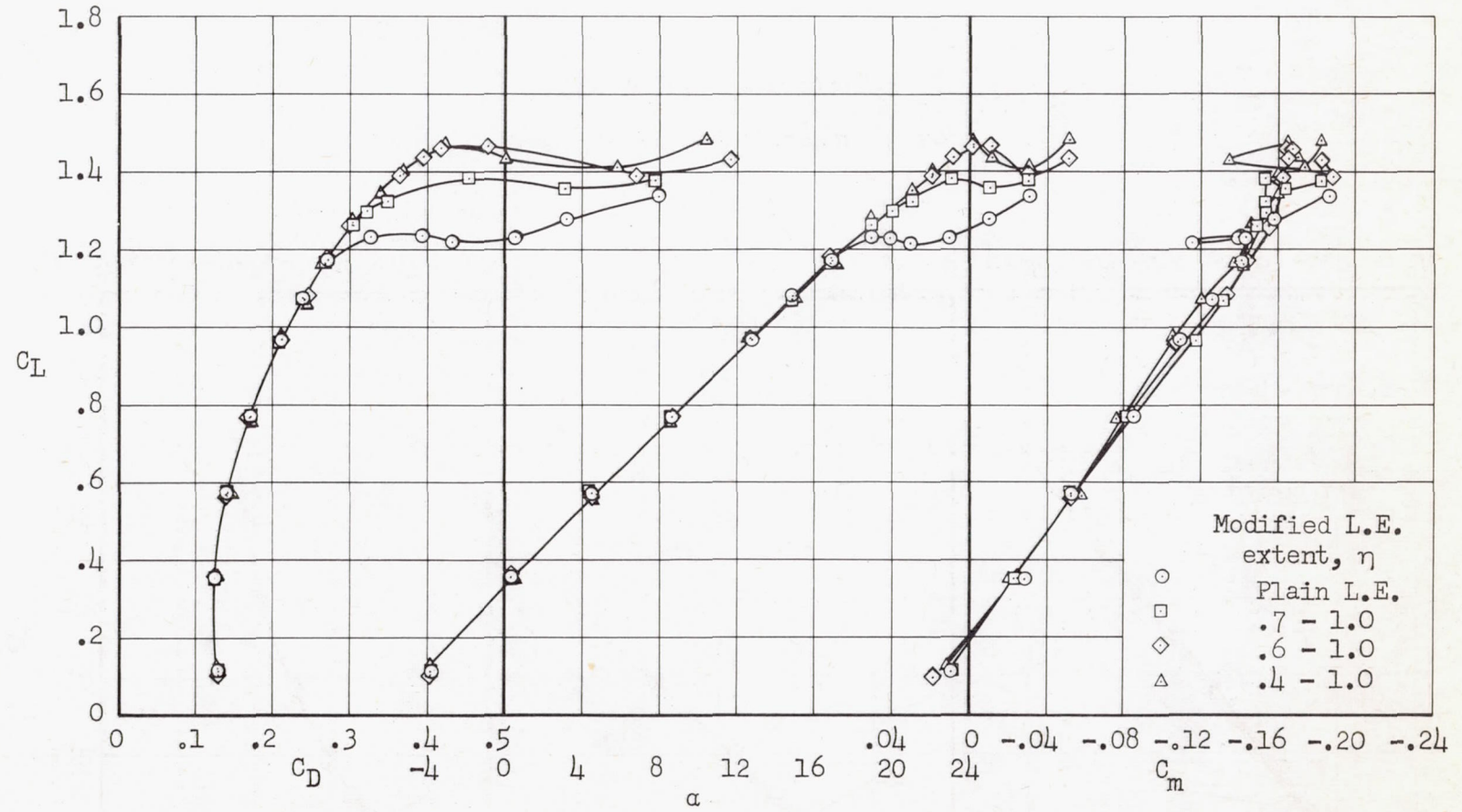
Figure 7.- Aerodynamic characteristics of the model with various amounts of leading-edge stall protection on the inboard portion of the wing ($\eta = 0.21 - 0.4$); small-span trailing-edge flap with suction; leading-edge flap suction ($\eta = 0.4 - 1.0$), $\delta_n = 50°$ ($\eta = 0.4 - 1.0$); modified leading edge ($\eta = 0.7 - 1.0$).
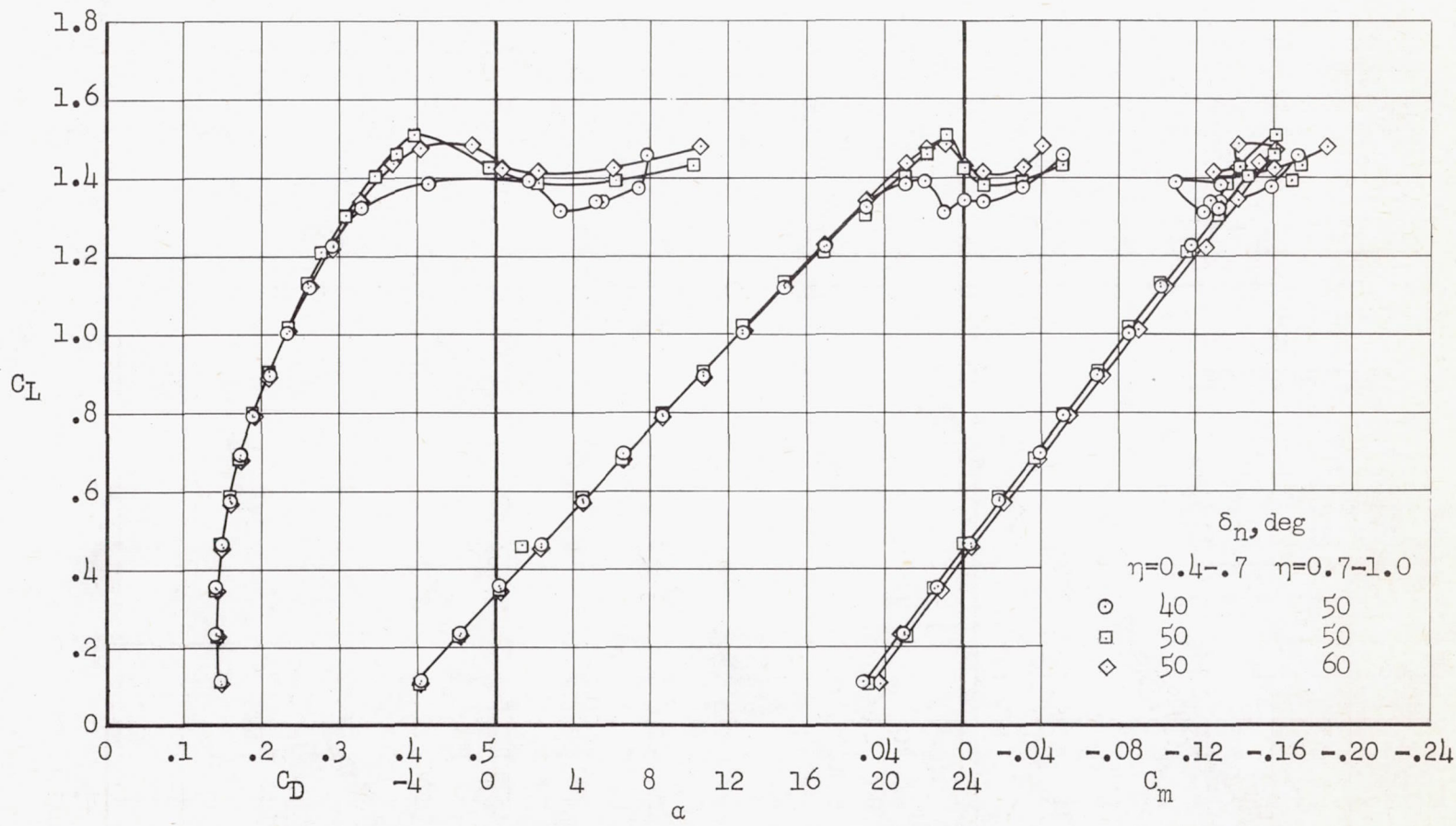
Figure 8.- Aerodynamic characteristics of the model with several outboard leading-edge flap configurations; small trailing-edge flap with area suction; leading-edge flap area suction (η = 0.4 - 1.0); δ_n = 30° for η = 0.21 - 0.4; modified leading edge (η = 0.7 - 1.0).
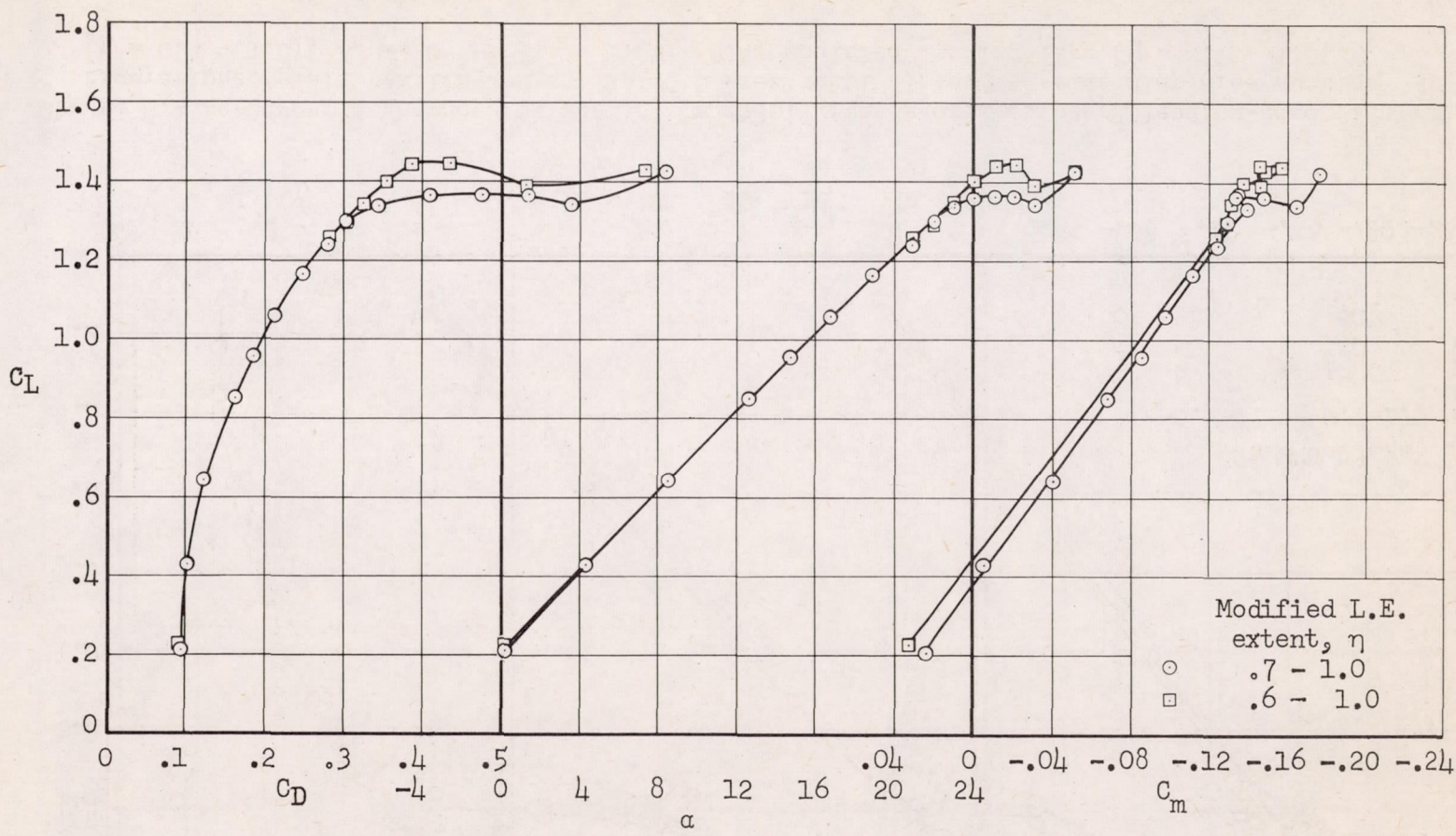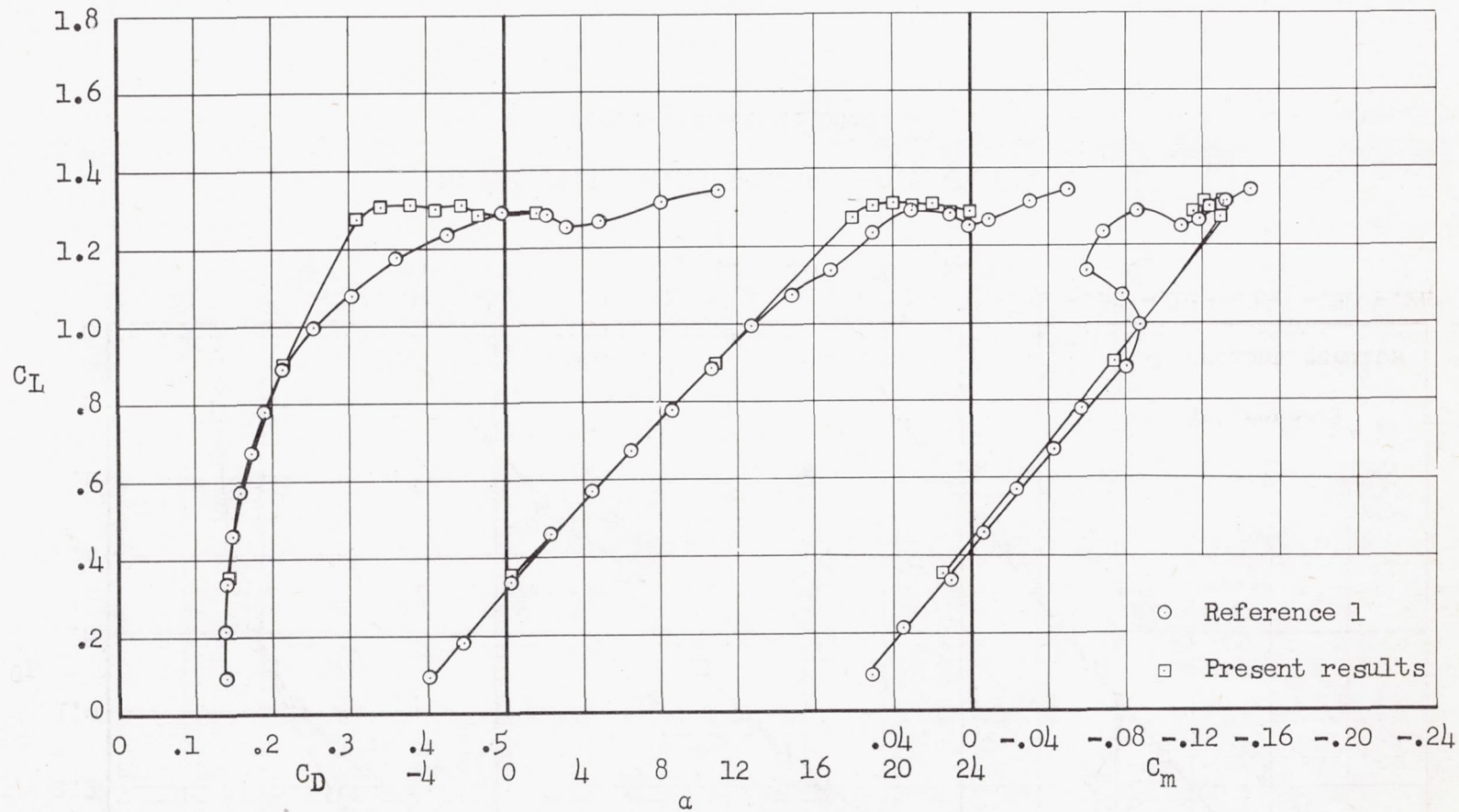
(a) Suction off (trailing-edge flap).

Figure 9.- Aerodynamic characteristics of the model with the small-span trailing-edge flap for several spanwise extents of the modified leading edge; leading-edge flap at 30°, 50°, 60°.
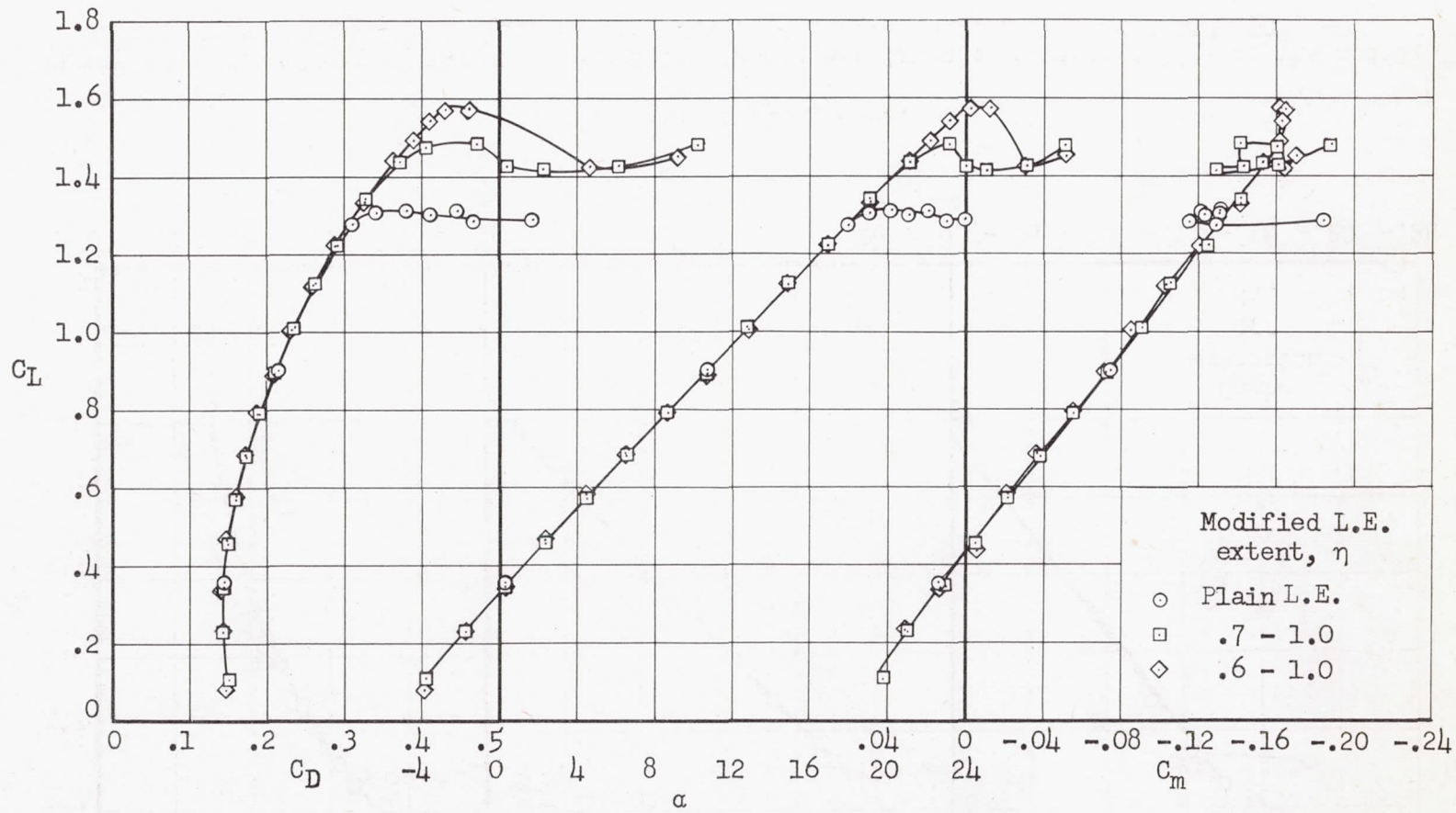
(b) Suction on (trailing-edge flap).

Figure 9.- Concluded.
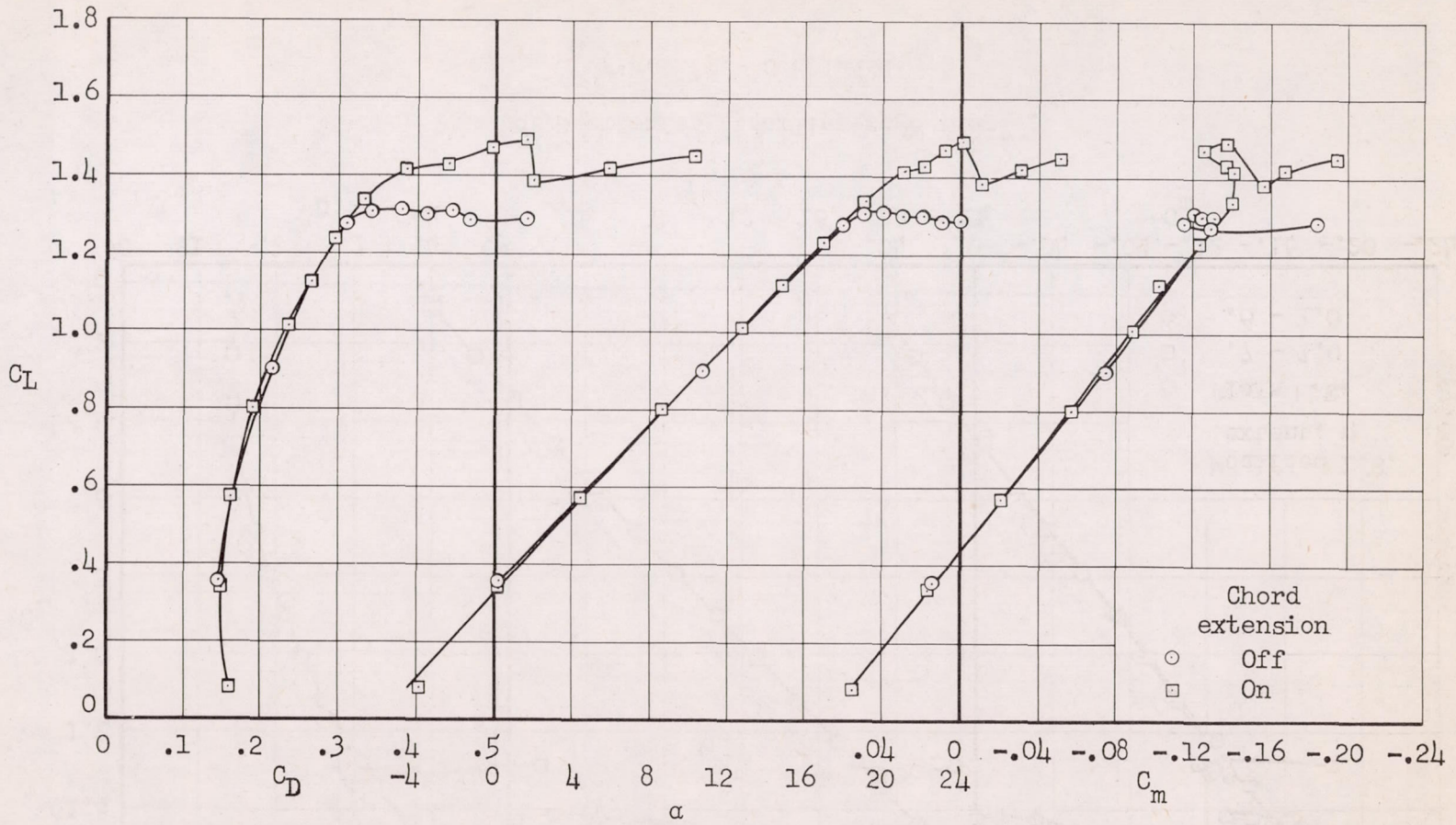
(a) Plain leading edge.

Figure 10.- The effect of the chord extension on the aerodynamic characteristics of the model; suction on the small-span trailing-edge flap; leading-edge flap deflected 30°, 50°, 60°.
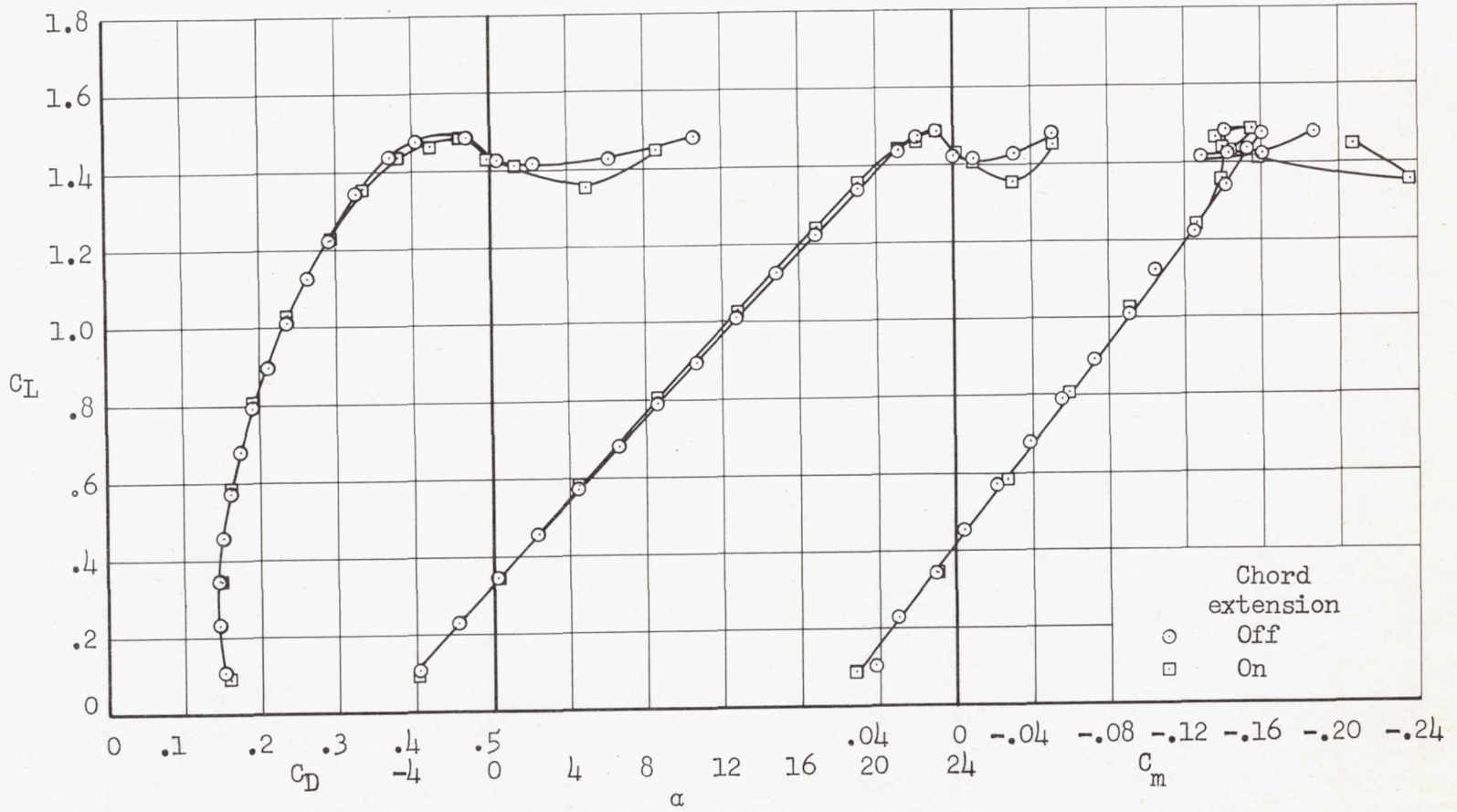
(b) Modified leading edge, $\eta = 0.7 - 1.0$.

Figure 10.- Continued.
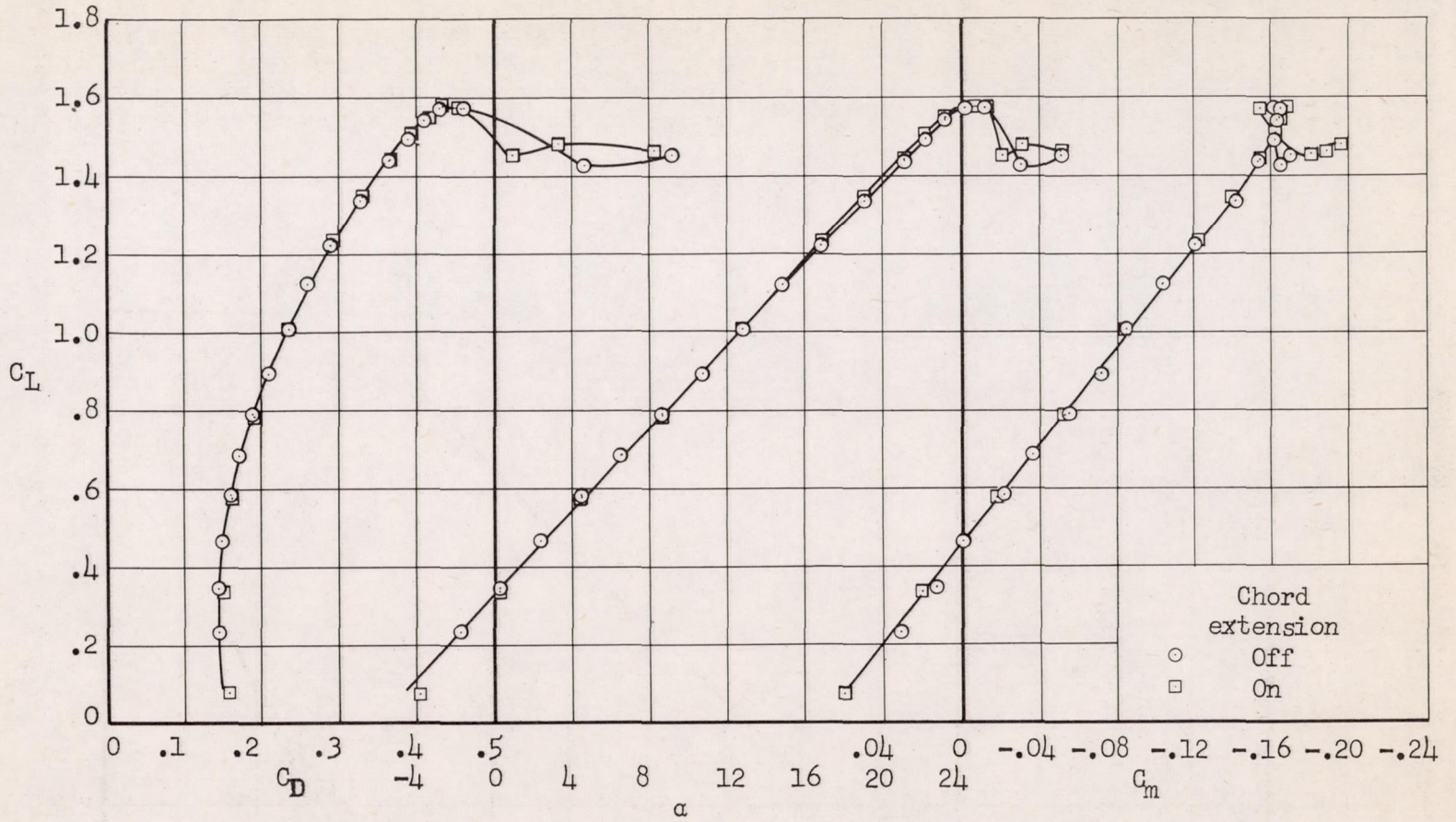
(c) Modified leading edge, η = 0.6 - 1.0.

Figure 10.- Concluded.
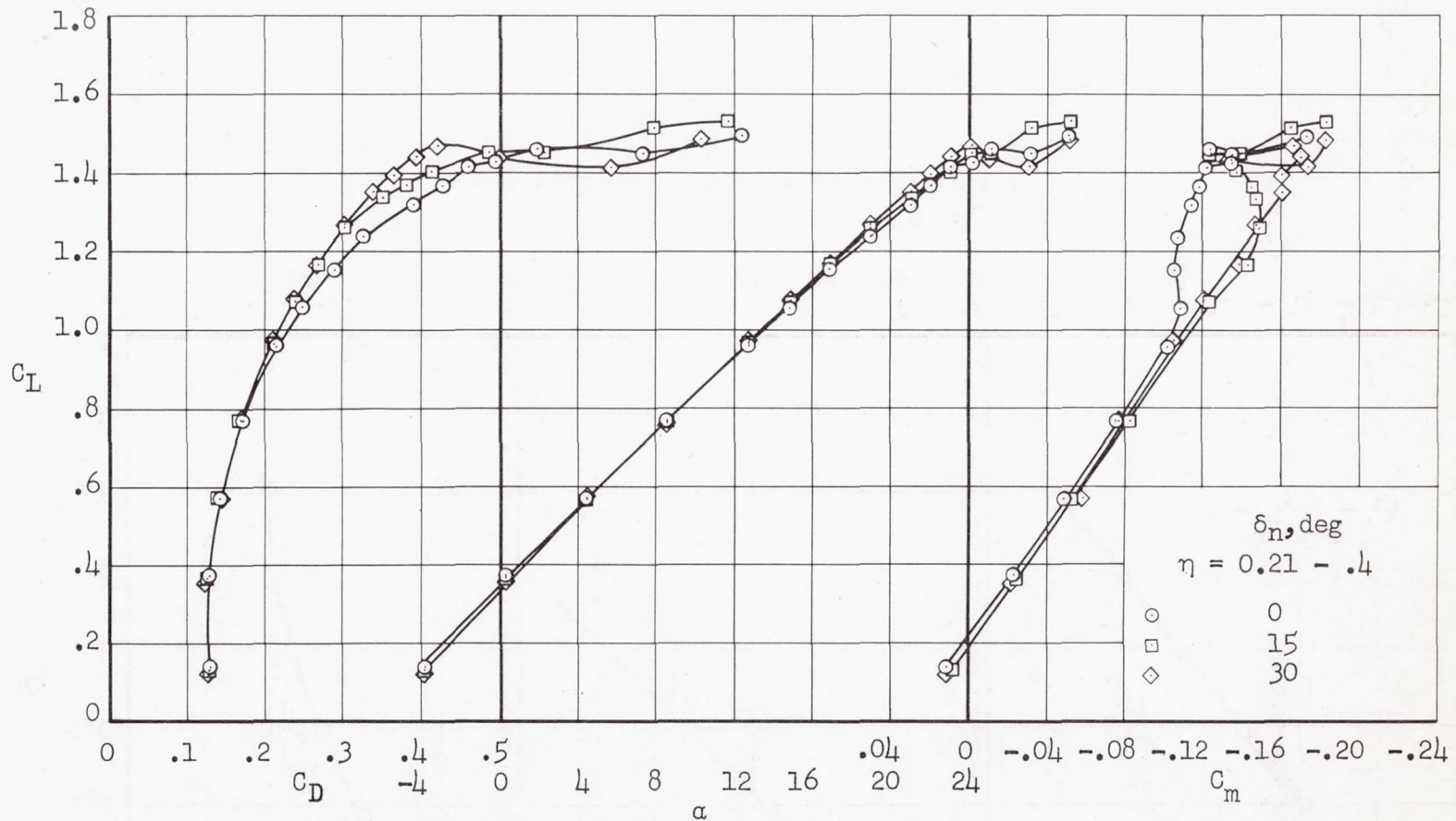
(a) Suction off (trailing-edge flap).

Figure 11.- Aerodynamic characteristics of the model with various amounts of leading-edge flap deflection on the inboard portion of the wing ($\eta = 0.21 - 0.4$); large-span trailing-edge flap deflected; leading-edge flap, $\eta = 0.4 - 0.7$, $\delta_n = 50°$; $\eta = 0.7 - 1.0$, $\delta_n = 60°$; area suction, $\eta = 0.4 - 1.0$; modified leading edge, $\eta = 0.4 - 1.0$.
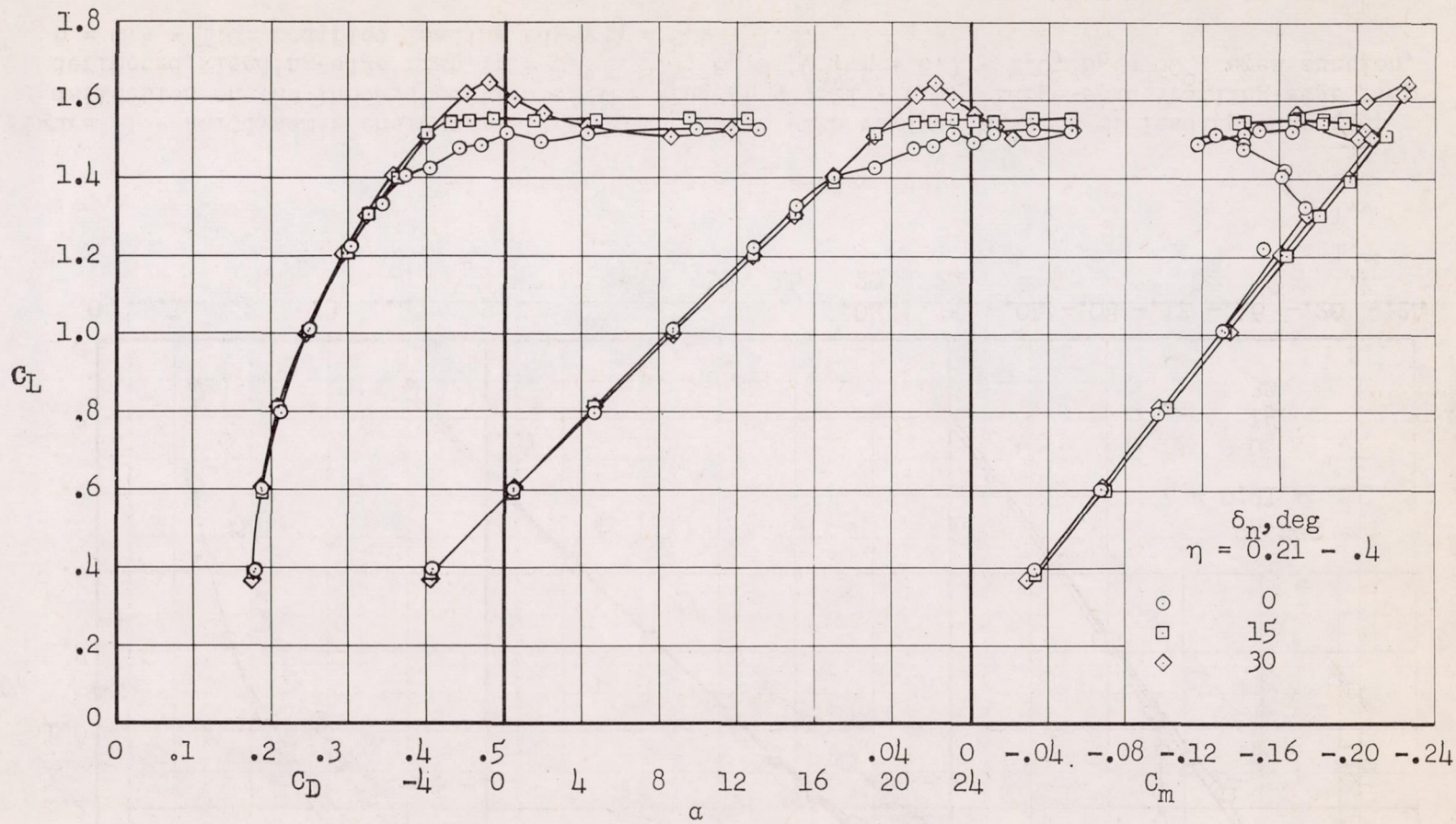
(b) Suction on (trailing-edge flap).

Figure 11.- Concluded.

(a) Suction off (trailing-edge flap).

Figure 12.- Aerodynamic characteristics of the model with the large-span trailing-edge flap for several spanwise extents of the modified leading edge; leading-edge flap at 30°, 50°, 60°.
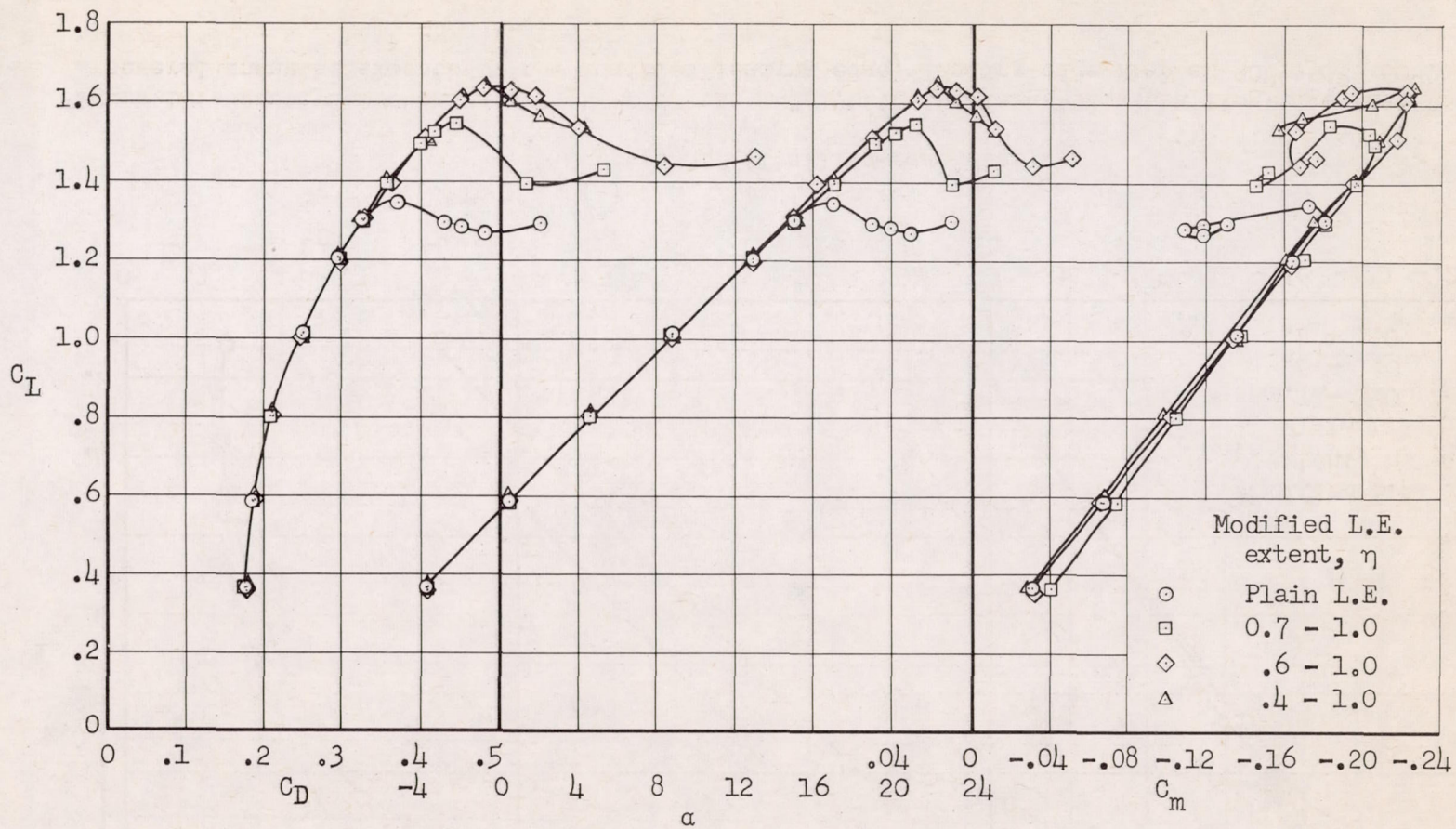
(b) Suction on (trailing-edge flap).

Figure 12.- Concluded.

(a) Plain leading edge.

Figure 13.- Aerodynamic characteristics of the model obtained with the most effective leading-
edge configurations used in both the present tests and those reported in reference 1; small-
span trailing-edge flap suction on; leading-edge flap (ref. 1) 0°, 40°, 40°, no suction,
and 30°, 50°, 60° with suction for present tests.
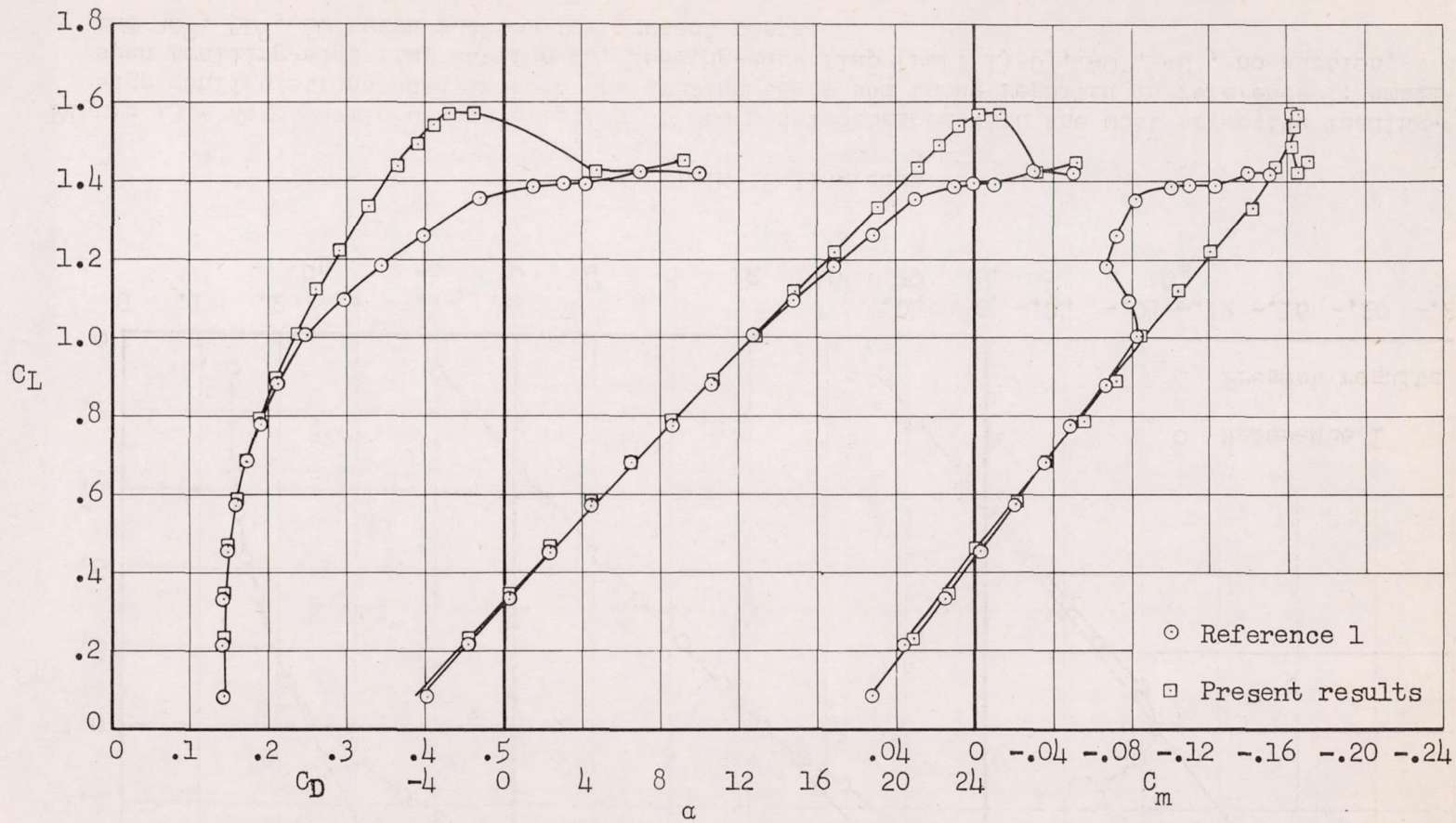
(b) Modified leading edge (η = 0.6 - 1.0).

Figure 13.- Concluded.
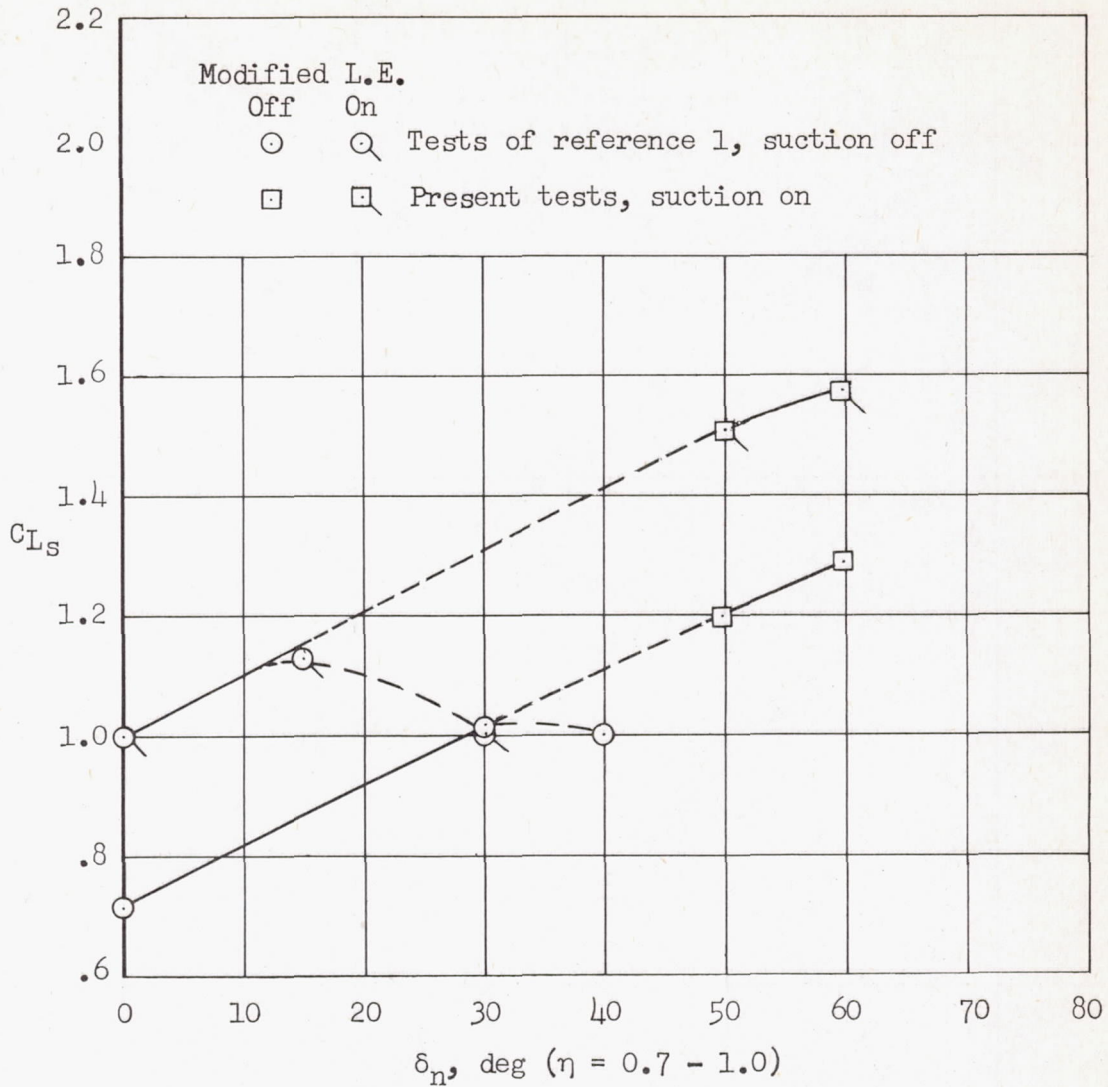
Figure 14.- The variation of the wing lift coefficient for tip stall with
  leading-edge flap deflection near the wing tip for the model with the
  small-span flap deflected.
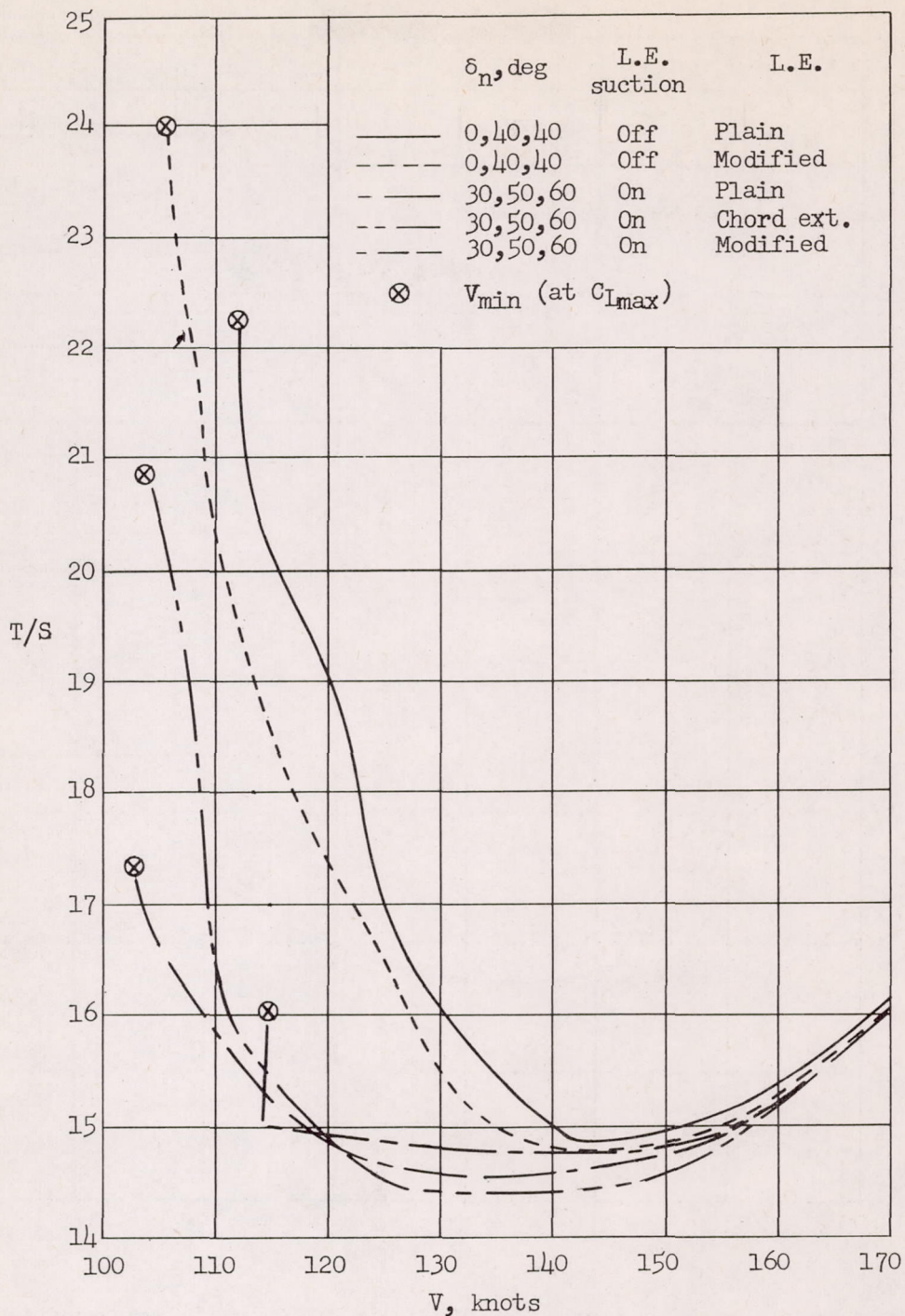
(a) Small-span flap.

Figure 15.- The variation of required thrust per unit wing area with airspeed for level flight; small-span flap with suction; $W/S = 60$.
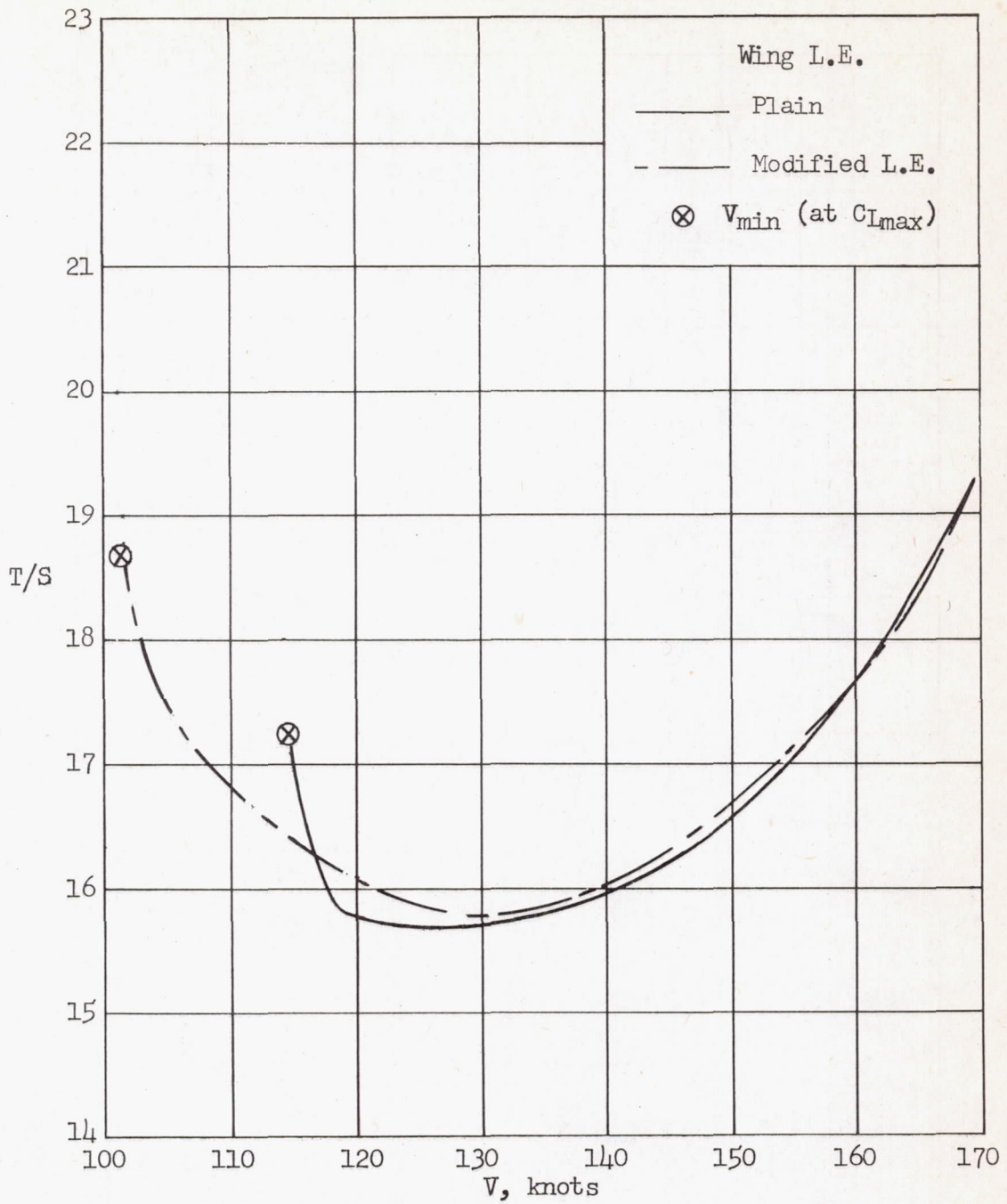
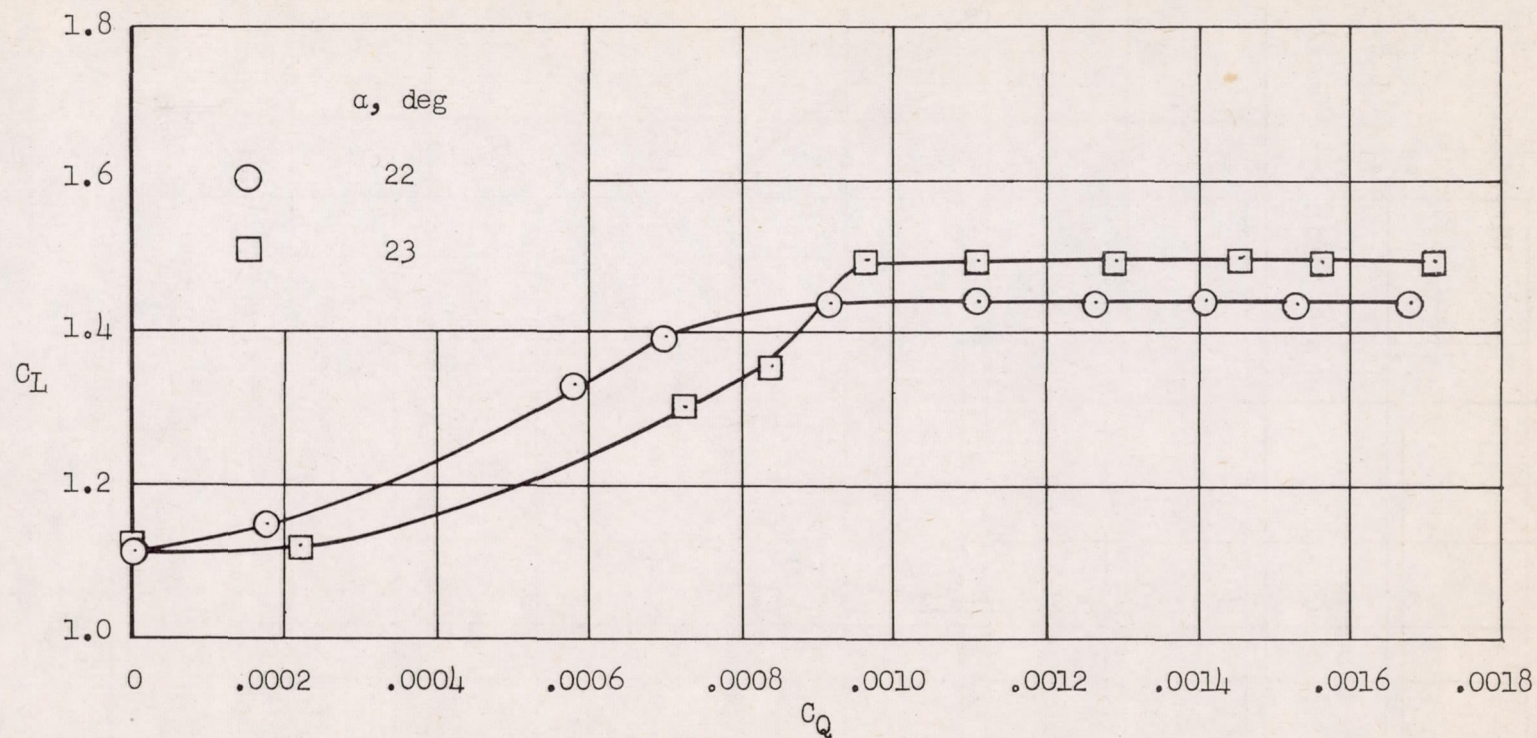(b) Large-span flap; leading-edge flap; 30°, 50°, 60° with area suction.

Figure 15.- Concluded.

Figure 16.- The effect of angle of attack near that of $C_{L_{max}}$ on the variation of C_L with C_Q; leading-edge flap, 30°, 50°, 50°; modified leading edge ($\eta = 0.7 - 1.0$); small-span trailing-edge flap; porous area 2.
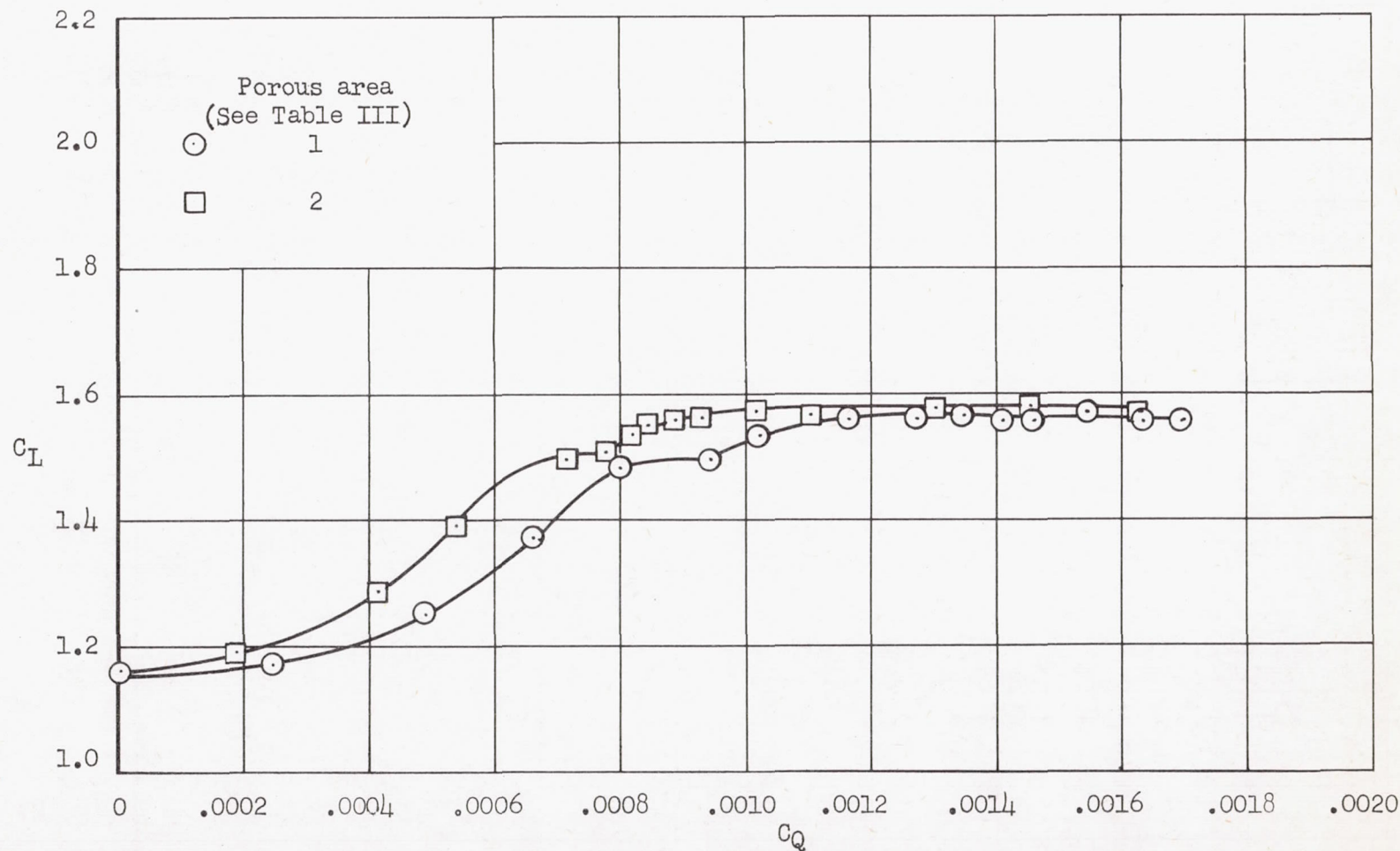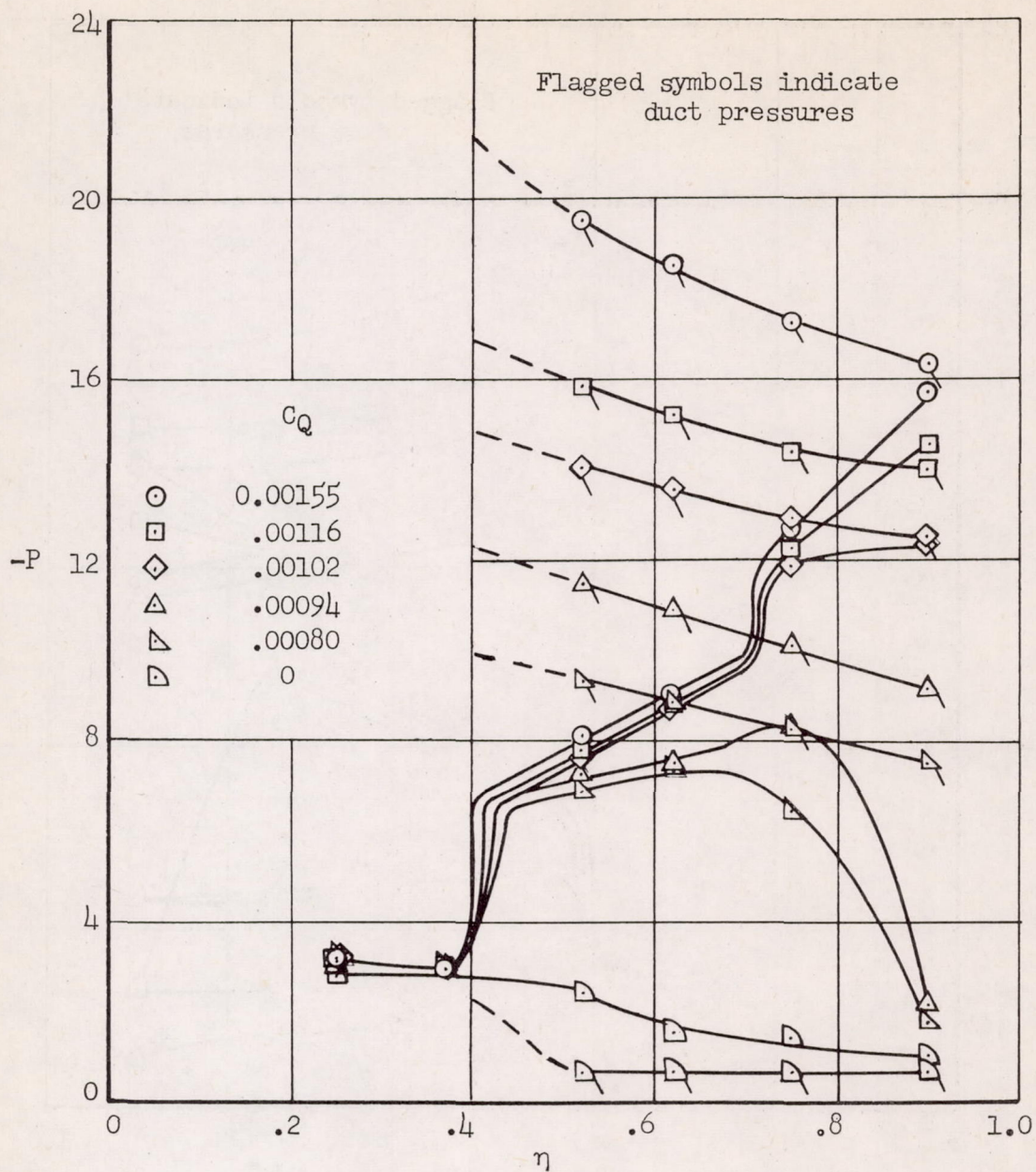
Figure 17.- The variation of lift coefficient with flow coefficient for two porous area configurations: leading-edge flap deflected 30°, 50°, 60°; modified leading edge, $\eta = 0.6 - 1.0$; small-span flap; $\alpha = 23°$.

(a) Porous area 1.

Figure 18.- The effect of flow coefficient and duct pressure on the span-
wise variation of minimum pressure at the leading-edge flap knee;
leading-edge flap deflected 30°, 50°, 60°; modified leading edge,
η = 0.6 - 1.0; small-span flap; α = 23°.
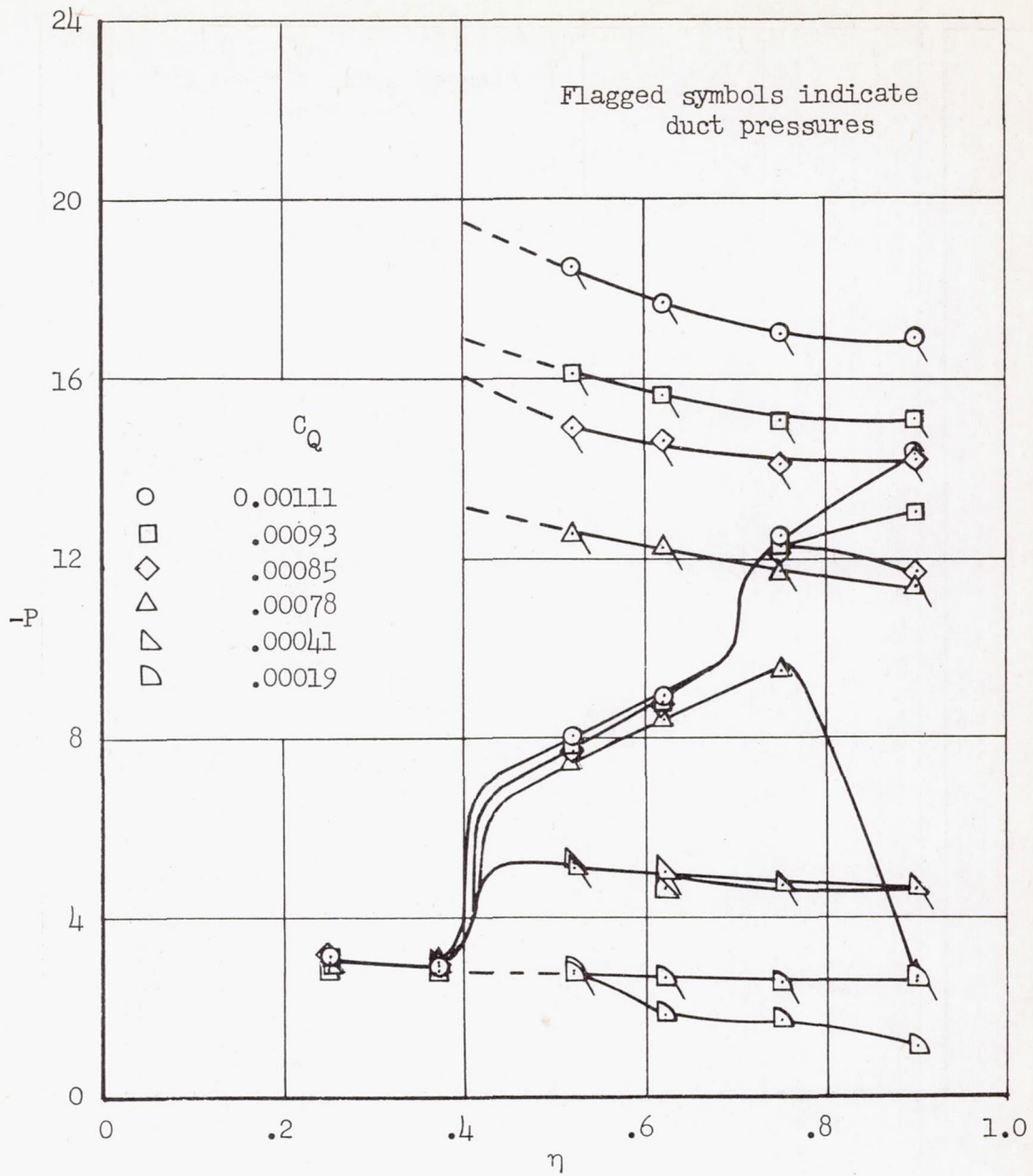
(b) Porous area 2.

Figure 18.- Concluded.